UNCLASSIFIED

SECURITY CLASSIFICATION AS...

(2)

AD-A212 119

DTIC ELECTE SEP 08 1989 S D

...DOCUMENTATION PAGE

Form Approved OMB No. 0704-0188

1a. REPORT SECURITY CLASSIFICATION	1b. RESTRICTIVE MARKINGS
2a. SECURITY CLASSIFICATION AUTHORITY	3. DISTRIBUTION/AVAILABILITY OF REPORT APPROVED FOR PUBLIC RELEASE DISTRIBUTION IS UNLIMITED
2b. DECLASSIFICATION/DOWNGRADING SCHEDULE	
4. PERFORMING ORGANIZATION REPORT NUMBER(S)	5. MONITORING ORGANIZATION REPORT NUMBER(S) AFOSR-TR- 89-1205
6a. NAME OF PERFORMING ORGANIZATION CORNELL UNIVERSITY	6b. OFFICE SYMBOL (If applicable)
6c. ADDRESS (City, State, and ZIP Code) ITHACA, NEW YORK 14853	7a. NAME OF MONITORING ORGANIZATION AFOSR/NA
	7b. ADDRESS (City, State, and ZIP Code) BUILDING 410 BOLLING AFB DC 20332-6448
8a. NAME OF FUNDING/SPONSORING ORGANIZATION AFOSR	8b. OFFICE SYMBOL (If applicable) NA
8c. ADDRESS (City, State, and ZIP Code) BUILDING 410 BOLLING AFB DC 20332-6448	9. PROCUREMENT INSTRUMENT IDENTIFICATION NUMBER AFOSR-87-0255
	10. SOURCE OF FUNDING NUMBERS PROGRAM ELEMENT NO. 61102F; PROJECT NO. 2307; TASK NO. A1; WORK UNIT ACCESSION NO.

11. TITLE (Include Security Classification)
GRANT AFOSR-87-0255, "VORTEX DYNAMICS"

89 9 074

12. PERSONAL AUTHOR(S)
LEIBOVICH, SIDNEY

13a. TYPE OF REPORT FINAL TECHNICAL REPORT	13b. TIME COVERED FROM 6/1/87 TO 5/31/89	14. DATE OF REPORT (Year, Month, Day) 1989, AUGUST 7	15. PAGE COUNT 94

16. SUPPLEMENTARY NOTATION

17. COSATI CODES			18. SUBJECT TERMS (Continue on reverse if necessary and identify by block number)
FIELD	GROUP	SUB-GROUP	
	20.04		AERODYNAMIC VORTICES; VORTEX BREAKDOWN; STABILITY; NONLINEAR TRANSITIONS,

19. ABSTRACT (Continue on reverse if necessary and identify by block number)

A theoretical description of vortex breakdown, suitable for design and control purposes, is under development. The objective is to incorporate the essential physical processes governing the occurrence, location, and strength of the phenomenon. It has been shown, under sponsorship of this grant, that the axisymmetric Euler equations possess solutions describing flow structures creating very strong disruptions of concentrated vortex flows having axial streaming. The nature of four classes of flow structures of this character have been described, and the interrelationships between them explained. Numerical analytical tools needed to treat the very large algebraic eigenvalue problems encountered in stability analyses of flows such as those found have been developed. In other tasks, (1) the linear instability characteristics of the Hall-Stewartson model of the leading-edge vortex have been determined asymptotically for large Reynolds numbers and (2) nonlinear transitions and mode interactions have been studied for viscous pipe flow.

20. DISTRIBUTION/AVAILABILITY OF ABSTRACT ☒ UNCLASSIFIED/UNLIMITED ☐ SAME AS RPT. ☐ DTIC USERS	21. ABSTRACT SECURITY CLASSIFICATION UNCLASSIFIED
22a. NAME OF RESPONSIBLE INDIVIDUAL LEONIDAS SAKELL	22b. TELEPHONE (Include Area Code) (202) 767-4935
	22c. OFFICE SYMBOL AFOSR/NA

DD Form 1473, JUN 86 — Previous editions are obsolete. — SECURITY CLASSIFICATION OF THIS PAGE

UNCLASSIFIED

Technical Objectives

This grant has as its goal the development of a theory of vortex breakdown capable of identifying the physical mechanisms responsible for the phenomenon, and upon which may be built practical methods of prediction and control of the phenomenon and its contribution to the forces and moments on aircraft and missiles. The two-year grant concluding May 31, 1989 initiated a systematic approach towards this ultimate goal in a multi-part program with more limited objectives.

- The first part, Task A, sought the construction of fully nonlinear axisymmetric solitary waves in vortices. This objective was identified in the expectation that the strong deceleration characteristic of vortex breakdown can be associated with large amplitude axisymmetric waves. This association provides a clear mechanism for the dominant features of vortex breakdown, and, since such waves were expected to be amenable to a relatively simple and compact mathematical representation, this provided the prospect of a kernel for rapid algorithms suitable for design or control purposes.

- The second part, Task B, sought ways to characterize the stability of the fully nonlinear solitary waves found in Task A to three-dimensional perturbations. It has been suggested (and laboratory experiments support the suggestion) that these large amplitude axisymmtric waves become unstable when they grow to some critical amplitude, and that this instability provides the mechanism to fix the equilibrium position and strength of a vortex breakdown structure.

- The third part, Task C, constituted a study of the linear stability of a mathematical model (due to Hall and Stewartson) of the leading edge vortex. The model leading edge vortex is explicitly known, and the objective of this part is to develop a simplified way to describe important instability mechanisms. The hope is that, once Task B is completed, simple descriptions, related to Task C, can be fitted to the instabilities of the large solitary waves that we expect to find. Simplification is expected to be important in designing rapid algorithms for design or control purposes.

- Because the general level of scientific understanding of nonlinear transitions in vortex flows having a component of velocity parallel to the vortex axis, as is the case in aerodynamic vortices, is virtually nonexistent, we undertook an additional study (Task D) on transitions in rotating Poiseuille flow. This flow, an exact solution of the Navier-Stokes equations, provides a convenient example to discover some of the important nonlinear dynamical features of vortices.

Other aspects governing the physics of vortex breakdown are of key importance, but were outside the scope of this two-year grant.

Status of the Research

Task A has been completed. Preliminary reports were given in [1] and [2], and a paper reporting the full details has been submitted for publication [3]. The manuscript for [3] is enclosed and is made part of this report by reference. The principal findings are that fully nonlinear solitary waves do exist, and that their properties are approximately captured by a remarkably simple ansatz. The paper also discusses large amplitude periodic wave trains, nonlinear deformations of vortex flows, and the interrelationships between these various classes of vortex flows. A more limited mathematical method also has been applied to this problem. A draft paper on this work exists ([4]): completion of this paper was consciously delayed partly because numerical work (since done) was thought desirable to make the findings of [4] more concrete, but more importantly because the work [3] was given a higher priority. We plan to finish and submit [4] for publication.

Task B is in progress. The mathematical problem to be solved here is a linear eigenvalue problem for a set of partial differential equations in three space dimensions. The problem is not separable, so the standard normal mode analysis technique of hydrodynamic stability theory does not apply. Because the numerical problem to be solved is extremely large, an attack on the problem capable of resolving the physically important scales required the development of new numerical techniques to solve large algebraic eigenvalue problems. The lack of efficient methods to accomplish this has been a stumbling block in the past. Under Task B, such methods have been developed, and a report on the algorithms developed is given in [5], which is also enclosed and incorporated in this report by

reference. Results using these numerical techniques on the stability problem were not available by the termination of the reporting period.

Task C is partially completed. Our work on the Hall-Stewartson model of the leading edge vortex has addressed the large Reynolds number limit, for which we have detailed the existence of unstable modes. This work was first reported in [6]. A draft of a paper [7] with a full description has been prepared. We have not yet found the critical Reynolds number for the onset of instability, since this requires a more extensive numerical effort.

Task D is partially completed. One paper describing mathematical aspects of the rotating Poiseuille (pipe) flow exists in draft form ([8]) and will soon be submitted for publication. Other work, detailing the nature of transitions and mode interactions has been done and has been briefly reported ([9]). The latter work traces a series of transitions in rotating pipe flows to chaotic states, and a paper will be written to report that investigation. We also have started, but not yet completed, work on three wave resonant interactions in rotating pipe flows.

Publications, Papers in review, Papers in Preparation

[1] S. Leibovich, Fully nonlinear structures, wavetrains, and solitary waves vortex filaments. In *Nonlinear Wave Interactions in Fluids*, ed. by R.W. Miksad, T.R. Akylas, & T. Herbert, AMD-Vol.87, Amer. Soc. Mech. Eng., 1987, pp.67-70.

[2] A. Kribus & S. Leibovich, Fully nonlinear waves on vortices, *Bull. Amer. Phys. Soc.*, (Abstract Only.)

[3] S. Leibovich & A. Kribus, Large amplitude wavetrains and solitary waves in vortices. Submitted to *J.Fluid Mech.*.

[4] S. Leibovich & A. Kribus, Monotone solutions for flows branching from columnar vortices. In preparation. Likely journal, *Acta Mechanica.*

[6] Z. Yang, S. N. Brown, & S. Leibovich, "Linear Instability of the Hall - Stewartson Model of Leading Edge Vortex", *Bull. Amer. Phys. Soc.*, (Abstract Only.)

[7] S.N. Brown, Z. Yang & S. Leibovich, On the linear instability of the Hall-Stewartson model of the leading edge vortex. In preparation. Likely journal, *J. Fluid Mechanics.*

[8] A. Mahalov, E.S. Titi & S. Leibovich, On invariant helical subspaces of the Navier-Stokes equations. In preparation. Likely journal, *Archives for Rational Mechanics & Analysis.*

[9] A. Mahalov & S. Leibovich, Nonlinear mode competition leading to chaos in rotating Hagen-Poiseuille flow. Planned paper. Likely journal, *J. Fluid Mechanics*.

Participating Professionals

Sidney Leibovich, Samuel B. Eckert Professor of Mechanical and Aerospace Engineering, Cornell University.

Susan N. Brown, Professor of Mathematics, University College, University of London.

Mr. Abraham Kribus, Ph.D. candidate, Cornell University.

Mr. Yang Zhigang, Ph.D. candidate, Cornell University.

Mr. Alexander Mahalov, Ph.D. candidate, Cornell University.

Interactions

Technical Meetings

American Physical Society Division of Fluid Mechanics, Eugene, OR, November 23, 1987, "Fully nonlinear structures, wavetrains and solitary waves in inviscid vortices" (A. Kribus, A. Szeri, & S. Leibovich)

American Society of Mechanical Engineers, Winter Annual Meeting, Boston, December 13-18, 1987. "Fully nonlinear structures, wavetrains, and solitary waves in vortex filaments". S. Leibovich. Invited Paper.

American Physical Society Division of Fluid Mechanics, Buffalo, NY, November 20, 1988. "Linear Instability of the Hall - Stewartson Model of Leading Edge Vortex". (Z.Yang,S. N.Brown, & S. Leibovich)

American Physical Society Division of Fluid Mechanics, Buffalo, NY, November 20, 1988. "Amplitude Expansion for Viscous Rotating Pipe Flow Near a Degenerate Bifurcation Point (A. Mahalov & S. Leibovich)

American Physical Society Division of Fluid Mechanics, Buffalo, NY, November 22, 1988. "Fully Nonlinear Waves on Vortices" (A. Kribus & S. Leibovich)

Seminars

"Static bifurcations of vortex flows", Department of Mechanical Engineering, Yale University, September 30, 1987. (S. Leibovich. Invited)

"Fully nonlinear wavetrains and solitary waves in inviscid vortices", NASA Ames Research Center, November 16, 1987. (S. Leibovich. Invited)

"Static bifurcations from columnar vortices", Department of Theoretical and Applied Mechanics, Cornell, Dec. 2, 1987. (S. Leibovich. Invited)

"Vortices, nonlinear waves, and vortex breakdown" , Arizona State University Department of Mechanical & Aerospace Engineering, March 24, 1988. (S. Leibovich. Invited)

"The Phenomenon of Vortex Breakdown", University of Minnesota Department of Aerospace Engineering and Mechanics, November 4, 1988. (S. Leibovich. Invited)

"The Vortex Breakdown Process", George W. Woodruff School of Mechanical Engineering, Georgia Institute of Technology, November 11, 1988. (S. Leibovich. Invited)

"Static Bifurcations of Vortices, and a Peek Beyond", Center for Fluid Dynamics, Turbulence, and Computation, Brown University, April 4, 1989. (S. Leibovich. Invited)

LARGE AMPLITUDE WAVETRAINS AND SOLITARY WAVES IN VORTICES

by
S. Leibovich & A. Kribus
Sibley School of Mechanical & Aerospace Engineering
Upson Hall, Cornell University
Ithaca, New York 14853-7501

Submitted to the *Journal of Fluid Mechanics*

Abstract

Large-amplitude axisymmetric waves on columnar vortices, thought to be related to flow structures observed in vortex breakdown, are found as static bifurcations of the Bragg-Hawthorne equation, equivalent to the steady, axisymmetric, Euler equations. Non-trivial solution branches bifurcate as the swirl ratio (the ratio of azimuthal to axial velocity) changes, and are followed into strongly nonlinear regimes using a numerical continuation method. Four types of solutions are found: multiple columnar solutions, corresponding to Benjamin's "conjugate flows", with subcritical-supercritical pairing of wave characteristics; solitary waves, extending previously known weakly nonlinear solutions to amplitudes large enough to produce flow reversals similar to the breakdown transition; periodic wavetrains; and solitary waves superimposed on the conjugate flow that emerge from the periodic wavetrain as the wavelength or amplitude becomes sufficiently large. Weakly nonlinear soliton solutions are found to be accurate even when the perturbations they cause are fairly strong.

1. Introduction

This paper is concerned with axially symmetric standing wavetrains and solitary waves, without restriction to infinitesimal or weakly nonlinear amplitudes, in inviscid incompressible vortex flows. Although the paper may be regarded strictly as a contribution to understanding of waves which may propagate on vortex cores, our motivation is the exploration of a conceptual picture of vortex breakdown given by Leibovich (1983) (and in a more widely accessible review in 1984, we shall designate either of these references as ***L***).

In aerodynamic contexts, the global flowfield causes impressed forcing on concentrated vortices embedded in it. Generally, the spatial scales of the forcing are large compared to scales associated with the vortex core. A conceptual model of vortex breakdown is promulgated in ***L***, guided in part by laboratory experiments and in part by the weakly nonlinear "trapped wave" theory of Randall and Leibovich (1973; or RL). In the scenario outlined in ***L***, vortex breakdown is a process that involves a crucial admixture of a strongly nonlinear axisymmetric wave propagating in a vortex "waveguide" having axially varying characteristics (and hence an axial pressure gradient), and a smaller asymmetric perturbation arising from instability of the big wave. The pressure gradient impressed by the waveguide does work on the axially symmetric wave, causing it to grow to large amplitude. The weakly nonlinear trapped wave theory of RL indicates that wave growth of this sort leads to a positional instability of the wave, as it grows, it propagates faster, and an equilibrium position cannot be established (with respect to a reference frame fixed by the waveguide) *unless there is a mechanism for extraction* of energy from the axisymmetric wave. RL invoked viscosity as a mechanism to dissipate wave energy. On the other hand, laboratory experiments (such as those done by Sarpkaya, 1972 and by Faler and Leibovich, 1977, 1978) show clear evidence of nonaxisymmetric features within a nearly axisymmetric "bubble" form of vortex breakdown, and the onset of asymmetry is consistent with an instability of the axially symmetric flow. If the "bubble" were regarded as a manifestation of a large amplitude, nearly axisymmetric, wave, then instability to asymmetric perturbations offers the possibility of much larger energy transfers from the wave than would viscous dissipation. Furthermore, the features of vortex breakdown appear to depend little on viscosity, at least at higher values of the Reynolds number. Consequently, it is suggested in ***L*** that the required energy extraction from the strongly nonlinear axially symmetric wave arises by the transfer of its energy to azimuthally asymmetric modes of motion which arise by instability. (It is pointed out in ***L*** that a large amplitude axially symmetric mode - large amplitude implying a variation occuring on axial scales comparable to the vortex core radius - is required in vortex breakdown, since only this component of a Fourier decomposition in the azimuth can lead to the deceleration of fluid on the vortex axis that is the hallmark of vortex breakdown.) On the basis of their experimental observations in flows very different from those already cited, Maxworthy, Mory, and Hopfinger (1983) also suggest, in a paper published in the same 1983 volume as the paper by Leibovich, that breakdown is associated with loss of stability of large axially symmetric waves to nonaxisymmetric perturbations.

To explore this suggested process, we have divided it into elements which at a later time must be recombined. The first element is the large amplitude axially symmetric wave, and the the aim of this paper is to develop a better understanding of these waves. The other ingredients of the hypothesis, not yet considered, are loss of stability to asymmetric perturbations, and effects engendered by axial inhomogeneity caused by the global flowfield.

In axially symmetric steady flow, it is well known that the Euler equations for inviscid swirling flow may be reduced to a single elliptic partial differential equation for the streamfunction. This equation seems to have been first discovered by Bragg and Hawthorne (1950), and in this paper we will refer to it by their names. Following Leibovich, 1985, we parameterize the Bragg-Hawthorne equation (BHE) by the relative level of the swirl, and construct standing waves, either infinite wavetrains or solitary waves, by studying the branching behaviors which arise as the parameter is varied (other, nonwavy flows, were discussed by Leibovich, 1985, from this starting point, and a few of the results to be detailed here for weakly nonlinear wavy flows were announced in Leibovich, 1987). The procedure can therefore be described as a search for static bifurcations of the BHE. Another natural parameterization that might have been chosen as a starting point for a bifurcation analysis is the wave speed of waves of permanent form. Here one adds a constant parameter to the primary axial velocity profile, given in a specific frame of reference, and regards the swirl as fixed. This choice, although more useful for some purposes than the parameterization using swirl level, introduces the wave speed parameter into the problem in an awkwardly nonlinear way, and we have not made use of it in this work.

Branching, when it occurs, is from a primary columnar vortex, assumed to be given. The flows which bifurcate from this vortex are required to have the same volume flow rate, and the same total head and circulation variation with streamfunction as does the given vortex. With these constraints and the assumption that the flow is either periodic in the axial direction with a finite wavelength L or is columnar at upstream and downstream infinity, we find that new flow branches may be of four kinds. One class (I, discussed in §4) of bifurcating flows is again columnar, so there are no axial variations; a second class (II, §6) consists of solitary waves with the primary flow at upstream infinity; periodic wavetrains comprise the third class (III, §5); and a fourth class (IV, §5) consists of solitary waves that approach a columnar flow at large axial distances that is distinct from the primary columnar flow.

The columnar branches, of which there is an infinite number, when taken together with the primary flow, are the "conjugate" flows defined and discussed in Benjamin's (1962) seminal paper. Two of these are especially important and receive emphasis in Benjamin's work; these are the primary flow, and what we shall call the principal conjugate flow, which is the columnar flow branching at the principal, or lowest, eigenvalue of the linearized problem, and therefore differing from the primary flow by an azimuthal vorticity that does not change sign. The procedure adopted here allows one to determine how these flows are connected together. We are also able to show that, at a columnar-columnar bifurcation point between the primary flow and its principal conjugate, there is a transfer of

Benjamin's (1962) criticality classification of the flows. That is, if one flow is supercritical on one side of the bifurcation point (does not admit upstream propagating waves of infinitesimal amplitude, and shorter standing waves), then the other columnar branch is subcritical (admits upstream propagating waves), and that these properties of the branches are exchanged as the bifurcation point is passed. (N.B. We use some of the language of bifurcation theory, but our use of the terms 'supercritical' and 'subcritical' is according to Benjamin's wave classification, and is not related to the direction of bifurcation.)

Fully nonlinear solutions have been determined numerically. This of course requires that specific examples of primary vortices be considered. We have chosen one family of examples, uniform axial velocity and the Burgers vortex. While the uniform axial velocity of this primary vortex differs from the jet-like or wake-like character of flows in which vortex breakdowns have been observed, the principal columnar flows which bifurcate from our example are either jet-like or wake-like depending on swirl level, and therefore closely resemble flows upstream or downstream, respectively, of vortex breakdown. In addition to the general results on columnar branches already mentioned, we note here an interesting - though academic - feature of the principal columnar branch. We have found that this branch can be numerically continued to very small swirl levels. With this clue as a point of departure, we show (in §4.4) the limit of vanishing swirl by asymptotic means, showing that continuation to zero swirl is possible.

Numerical examples of fully nonlinear wavy solutions similar to some of those discussed in this paper have been presented by Hafez et al. (1986) (an abbreviated account is given by Hafez and Salas, 1985). Our paper gives a considerably more comprehensive picture of the inviscid picture by identifying classes of solutions other than periodic wavetrains, and by uncovering the connections between them. The results of Hafez et al. were computed for a different (although more or less similar) class of primary vortices, yet their results are qualitatively similar to ours. This, and the theoretical argument of this paper, leads us to believe that the response to variation of swirl, and the main characteristics of the flows to be described here, are not the consequence of a special choice of profiles for the numerical work, but are of general applicability.

Solitary waves of class II can be found for the supercritical values of parameter by numerically continuing known weakly nonlinear solitary waves (with our choice of primary vortex, we have access to weakly nonlinear results found by Leibovich, 1970, which we use as a starting point) to large amplitude. These solitary wave flowfields approach the primary columnar flow asymptotically at large upstream and downstream distances. Their amplitudes can be increased to values sufficiently large to cause stagnation points to appear, followed by encapsulated regions of closed streamlines. The utility of the results when flow reversals are present requires careful consideration, particularly since added nonuniqueness enters in such circumstances, and the consistency requirement of the Prandtl-Batchelor criterion is violated. We believe that the results will prove to be of value at these large amplitudes, and discuss the reasons for this belief in the final section (§7). An interesting and potentially useful point is that even at amplitudes large enough to cause stagnation and reversed flow, the weakly nonlinear solitary wave solutions remains an good approximation to the results of the fully nonlinear calculations.

For subcritical parameter values, periodic wavetrains (class III) have been found by numerical continuation beginning with infinitesimal waves. As the amplitudes of the periodic wavetrains increase at fixed wavelength in the numerical examples (as they do when the parameter measuring swirl increases), the wave troughs become highly localized, and the wave crests become very broad. These broad crests have virtually no axial variation, that is, they are nearly columnar. We show that these nearly columnar flow closely approximate, at large wave amplitude, the columnar principal conjugate vortex. The same kind of behavior is found to hold when the swirl level is held fixed, but the wavelength of a wavetrain is increased. In either case, an individual wave trough approaches a solitary wave with the principal conjugate columnar vortex being the flow at "large" distances upstream and downstream. Thus, we are led to another family of solitary waves (class IV) distinct from those supported by the primary vortex, but clearly connected to it.

2. Problem formulation

The Euler equations in cylindrical coordinates (r,θ,z) for steady, incompressible, axially-symmetric flow may be reduced to a single elliptic partial differential equation for the Stokes streamfunction, ψ, related to the radial (u) and axial (w) by

$$u = -r^{-1}\psi_z \ , \ w = r^{-1}\psi_r \ .$$

The equation, which connects the azimuthal vorticity to the total head and circulation, seems to have been first found by Bragg and Hawthorne (1950) and is given by

$$D^2\psi = r^2 H'(\psi) - FF'(\psi) \qquad \text{(BHE)}$$

where

$$D^2\psi \equiv \psi_{rr} - (1/r)\,\psi_r + \psi_{zz} \ ,$$

is $-r^{-1}$ the azimuthal component of vorticity. A number of other authors have made use of this equation notably Long (1953), Frankel (1956), Squire (1956), and Benjamin (1962). See Batchelor (1967) for a convenient reference for a derivation of BHE, following Bragg and Hawthorne, or Yih (1965) for a derivation by an alternate method. The replacement of the Euler equations by BHE is justifiable at all points in a steady, inviscid and axially symmetric flow with the possible exception of meridional stagnation points (i.e., where $u = w = 0$, but v, the azimuthal velocity component, may be nonzero), which are singular points of the transformation. In BHE, $H(\psi)$, the total head or Bernoulli function

$$H(\psi) = \frac{p}{\rho} + (1/2)\, v \cdot v \,, \tag{1}$$

and $F(\psi)$, the circulation about the symmetry axis (apart from a factor of 2π),

$$F(\psi) = rv(r,z) \tag{2}$$

are functions of ψ alone. That F is a function of ψ alone is a consequence of conservation of angular momentum in an inviscid fluid.

Solutions to (BHE) are solutions to the Euler equations under the stated restrictions, and different inviscid flow problems arise from the specifications of the pair of functions H and F. The simplest cases are those for which the radial component of velocity vanishes at some plane $z = z_1$ on which the axial (w) and azimuthal (v) velocity components are specified to be W(r), V(r) with $W \neq 0$, then $H'(\psi)$ and F are easily determined (see Benjamin, 1962). In this case, which we consider here,

$$\frac{1}{\rho}\frac{\partial p}{\partial r} = \frac{V^2(r)}{r} \tag{3}$$

at this plane. Since

$$\psi(r,z_1) = \int_0^r rW(r)\, dr \equiv \Psi(r) \tag{4}$$

we can suppose this latter relation to be inverted to give

$$r = R(\psi) \tag{5}$$

This inversion can always be done (in principle) if $W(r) \neq 0$. At $z = z_1$, we can now regard W as a function of ψ, since

$$W = \frac{1}{r}\frac{d\psi}{dr}(r,z_1) = \frac{1}{R(\psi)}\frac{d\psi}{dR}(R(\psi)) \tag{6}$$

With V(r) prescribed, $F(\psi)$ is determined to be

$$rV \equiv F(\psi) = R(\psi)\, V(R(\psi)). \tag{7}$$

The pressure may now be found as a function of ψ from (3) by integration.

$$\frac{1}{\rho}p = \frac{1}{\rho}p(0,z_1) + \int_0^{R(\psi)} \frac{V^2(r)}{r}\,dr, \tag{8}$$

and thus $H(\psi)$ may be identified. If the radial velocity is not given to be zero at $z=z_1$, but is prescribed as some nontrivial function of r, a similar construction of $H(\psi)$, $F(\psi)$ can be carried out. We call the flow given at the plane $z=z_1$ the "specifying flow", this will be taken to be the basic, or primary, flow and the starting point of our investigations.

Only $H'(\psi)$ is required for the analysis, $H(\psi)$ itself is not needed. At a plane $z=z_1$ where $u = 0$, $v = V$, $w = W$, and

$$\frac{dH}{d\psi} = \frac{\partial H}{\partial r}\frac{dR}{d\psi} = \frac{1}{R^2}F\frac{dF}{d\psi} + \frac{1}{R}\frac{dW}{dR} \tag{9}$$

Now we suppose that, at $z = z_1$, the functional form of the swirl $V(r)$ is fixed, but the level is adjustable, so that

$$F(\psi) = \lambda f(\psi) \tag{10}$$

where f is a fixed function, and λ is an adjustable constant. Equation (BHE) for ψ may be written

$$D^2\psi = r^2A(\psi) - \lambda^2B(\psi,r^2) \tag{11}$$

where

$$A(\psi) = \frac{1}{R(\psi)}\frac{dW}{dr}(R(\psi)), \text{ and } B(\psi,r^2) = (R^2(\psi)-r^2)\,ff'(\psi)/R^2(\psi). \tag{12}$$

With the appropriate interpretation of λ, we may regard equation (11) as dimensionless. Thus, if we scale distances by a characteristic radius b (such as that of a bounding tube, or, alternatively, the location of the maximum swirl speed), the specifying axial velocity with a characteristic speed W_0 (such as its value on the axis), the streamfunction with b^2W_0, the azimuthal speed with a typical value V_0 (such as the maximum occuring in the flow), then

$$\lambda = \frac{V_0}{W_0}.$$

and we may interpret (11) as a dimensionless equation.

The parameter λ appears only as λ^2, and so we replace it hereafter with

$$\Lambda = \lambda^2, \tag{13}$$

and as a consequence of its definition, only admit positive values of Λ.

Suppose the boundaries of the fluid in the (r,z) plane have, as two constituents, the impermeable cylinders r = a and r = 1 > a (here we have chosen the outer tube radius as length scale for our problem). The columnar specifying flow

$$\psi \equiv \Psi(r) . \tag{14}$$

is a solution of (11) holding for all $\Lambda > 0$. We now wish to find other solutions, periodic in z with a prescribed wavelength L. Since both the specifying columnar flow and any other wave-like solutions that may exist simultaneously satisfy the same mathematical problem,and one possibility for this to occur is by bifurcation of new branches of solutions from the specifying flow, and the multiple solutions so obtained, when of small amplitude, may be identified as the waves propagating on the specifying flow previously found in the literature (cf. Long, 1953, Frankel, 1956, Squire, 1956, Benjamin, 1962). Let

$$\Phi = \psi - \Psi(r), \tag{15}$$

represent the perturbation streamfunction. If there are other solutions, there is a z-periodic nontrivial solution to the (elliptic) partial differential equation

$$N(\Phi,\Lambda) = D^2\Phi + \Omega(\Phi,r,\Lambda) = 0 \tag{16a}$$

where

$$\Omega(\Phi,r,\lambda) = \Lambda P(\Phi,r) - r^2 Q(\Phi,r) \tag{16b}$$

with $P(\Phi,r) \equiv B(\Psi + \Phi, r^2) - B(\Psi, r^2)$

and $Q(\Phi,r) \equiv A(\Psi + \Phi) - A(\Psi)$

satisfying the boundary conditions

$$\Phi(a,z) = \Phi(1,z) = 0, \tag{16c}$$

$$\Phi(r,z - \tfrac{1}{2}L) = \Phi(r,z + \tfrac{1}{2}L) \tag{16d}$$

The nonlinear problem admits solutions even in z, and we focus on these. In addition to admitting solutions with this symmetry ($z \to -z$), solutions are also admitted with $z \to z + h$, for any h. Thus, smooth z-periodic solutions may be constructed by appropriately piecing together (by reflections and shifts) solutions satisfying the Neumann boundary conditions.

$$\frac{\partial\Phi}{\partial z}(r,0) = \frac{\partial\Phi}{\partial z}(r,\tfrac{1}{2}L) = 0. \tag{16e}$$

3. Static bifurcation analysis

The Bragg-Hawthorne equation describes only steady, or 'static', solutions. It can therefore be used to describe branches of the families of steady solutions corresponding to the same functional forms (as functions of the streamfunction) for the total head and circulation, and the same volume rate of flow. The bifurcation and continuation of such branches is discussed in this section. The question of the stability of the various solution branches of the BHE is a dynamical problem. This cannot be answered in the context of the BHE equation, and it is necessary to return to the Euler equations in which solutions to BHE are embedded. This is addressed (for columnar solutions only) in §5.

3.1. Perturbation expansion

We know that the specifying flow, $\Phi \equiv 0$, is a solution to the problem (16) for any value of the parameter Λ. This can fail to be a unique solution branch for a given Λ only when $L(0,\Lambda)$, the operator defined by the linearization of $N(\Phi,\Lambda)$ about $\Phi = 0$, is not invertible. This occurs only when the parameter Λ coincides with an eigenvalue, μ (say), for the linearized problem

$$\begin{aligned} L(0,\Lambda)o_0 &\equiv D^2 o_0 + \frac{\partial\Omega}{\partial\Phi}(0,r,\Lambda)\, o_0 \\ &= D^2 o_0 + \left[\Lambda\frac{\partial P}{\partial\Phi}(0,r) - r^2\frac{\partial Q}{\partial\Phi}(0,r)\right] o_0 = 0. \end{aligned} \tag{17a}$$

$$o_0(a,z) = o_0(1,z) = 0, \quad o_0(a,z - \tfrac{1}{2}L) = o_0(a,z + \tfrac{1}{2}L). \tag{17b}$$

For Λ near an eigenvalue μ, we construct a solution branching from the specifying flow in a perturbation series. This will provide a local approximation for the solution branching at μ, which we will continue numerically to larger values of $|\Lambda - \mu|$. Let

$$\Phi = \varepsilon(\phi_0 + \varepsilon\phi_1 + \ldots) \tag{18a}$$

$$\Lambda(\varepsilon) = \mu + \varepsilon\kappa(\varepsilon) = \mu + \varepsilon(\kappa_0 + \varepsilon\kappa_1 + \ldots) \tag{18b}$$

and set

$$p_k(r) = \frac{1}{k!}\frac{\partial^k P}{\partial \Phi^k}(0,r), \tag{19a}$$

$$q_k(r) = \frac{1}{k!}\frac{\partial^k Q}{\partial \Phi^k}(0,r), \tag{19b}$$

$$s_k(r;\mu) = \mu p_k(r) - r^2 q_k(r), \tag{19c}$$

where μ refers to any eigenvalue of the linearized problem (17) and ϕ_0 the corresponding eigenfunction, ε is a small ordering parameter measuring the amplitude of the bifurcating solutions and the difference between Λ and its value μ at the bifurcation point, and the dots stand for higher order terms in ε. When these relationships are substituted into (16a), Taylor series expansions in powers of ε carried out and each coefficient in the series is set to zero, the first three coefficients are

$$L(0,\mu)\phi_0 = D^2\phi_0 + [\mu\, p_1(r) - r^2 q_1(r)]\phi_0 = 0 \tag{20a}$$

$$L(0,\mu)\phi_1 = -\{\kappa_0 p_1(r)\phi_0 + s_2(r;\mu)\phi_0^2\} \tag{20b}$$

$$L(0,\mu)\phi_2 = -\{\kappa_1 p_1(r)\phi_0 + \kappa_0 p_1(r)\phi_1 + \kappa_0 p_2(r;\mu)\phi_0^2 + 2s_2(r;\mu)\phi_0\phi_1 + s_3(r;\mu)\phi_0^3\} \tag{20c}$$

and all the ϕ_n satisfy the same boundary conditions (17b).

Note that

$$p_1(r) \equiv \frac{\frac{1}{r^3}\frac{df^2}{dr}}{W^2(r)}$$

and

$$q_1(r) \equiv \frac{1}{rW}\frac{d}{dr}\left(\frac{1}{r}\frac{dW}{dr}\right).$$

The numerator of $p_1(r)$, when multiplied by Λ, is Rayleigh's discriminant, and therefore sensible problems, in the context of considerations such as in this paper, will have $p_1(r) > 0$, and we assume this to be the case. (Otherwise, the primary flow is unstable.) Only positive values of μ can correspond to branch points, since $\Lambda > 0$ by definition. If $p_1(r) > 0$ and $q_1(r) \geq 0$, then the smallest (or "principal") eigenvalue is guaranteed positive (Leibovich, 1985), and is therefore a possible branch point. Positive values of $q_1(r)$ are not necessary for this to be so. In the development below, we tacitly assume the smallest eigenvalue is positive. If this is not so, then the mathematical changes needed are obvious - one deals only with the positive eigenvalues, of which there is an infinite number - but the branching solutions are likely to be unstable and therefore physically uninteresting.

The problems we have posed here depend on two parameters, Λ and L, once the specifying flow is selected.

The principal eigenfunction has no zeros in the interior of D (Courant and Hilbert, 1953), and without loss of generality, we therefore may take it to be nonnegative. Even eigenfunctions are all of the form

$$o_0 = \chi_{pm}(r)\cos(2m\pi z/L), \tag{21}$$

where the integer index p is the number of internal zeros of $\chi_{pm}(r)$, which satisfies the problem

$$(r\frac{d}{dr})(\frac{1}{r}\frac{d\chi_{pm}}{dr}) + [\mu_{pm}\, p_1(r) - r^2 q_1(r) - (\frac{2m\pi}{L})^2]\,\chi_{pm} = 0 \tag{22}$$

$$\chi_{pm}(a) = \chi_{pm}(1) = 0.$$

Here we have labeled the eigenvalues according to the indices p and m corresponding to the associated eigenfunction. The principal eigenfunction corresponds to m = 0 and to the index p, which we can take to be p = 0, such that the function $\chi_{00}(r)$ has no zeros internal to D. The principal eigenfunction belongs to the eigenvalue μ_{00} and is a function of r alone. A solution which branches from the principal eigenvalue therefore corresponds to a new columnar flow (which we will call the "principal conjugate branch" since it is a conjugate flow as defined by Benjamin, 1962), and an infinite number of other columnar flows (also conjugates in the sense of Benjamin) branch from larger eigenvalues corresponding to m = 0 and the eigenfunctions $\chi_{p0}(r)$, for p = 1,2,3,.... Solutions periodic in z (standing waves) branch from eigenvalues corresponding to eigenfunctions with $m \neq 0$. Modes for all values of m are characterized by the number of zeros of their eigenfunctions with $\chi_{pm}(r)$ having p internal zeros.

The eigenvalue problem (17) is in standard Sturm-Liouville form (Courant & Hilbert, 1953), and some of its features (such as bounds on the smallest eigenvalue) are discussed by Leibovich (1985). There is one comment which is worth making at this point about this eigensystem, in addition to the observations we have already made. Eigenvalues corresponding to z-dependent eigenfunctions (constituting "wavy" modes, with eigenvalues exceeding $\mu_{(0)}$), decrease as L increases (Courant & Hilbert, 1953), and as $L \to \infty$, $\mu_{(0)}$ is an accumulation point for the wavy eigenvalues μ_{0m}, $m \neq 0$. For the same reason, waves corresponding to higher radial modes have accumulation points, with $\mu_{pm} \to \mu_{p0}$ as $L \to \infty$.

3.2. Branching behavior

If ϕ_0 is an eigensolution, then the solution to the adjoint eigenvalue problem with an unweighted inner product is ϕ_0/r, or alternatively, the problem is self-adjoint under the inner product

$$(F,G) = \langle FG \rangle$$

where

$$\langle \bullet \rangle = \int_D r^{-1} (\bullet) dr\, dz,$$

and D is the spatial domain in which our problem is set.

For the problem for ϕ_1 to have a solution, the solvability condition

$$\kappa_0 = - \frac{\langle s_2(r;\mu)\phi_0^3 \rangle}{\langle p_1(r)\phi_0^2 \rangle} \tag{23}$$

must be satisfied. If $\mu = \mu_{(0)}$ is the smallest eigenvalue, then ϕ_0 is the primary eigenfunction, which may be taken to be positive. Unless $\mu_{(0)}p_2(r) - r^{-2}q_2(r)$ is distributed in a special way, then, κ_0 is nonzero and the bifurcation at $\mu_{(0)}$ occurs with finite slope (i.e., it is transcritical or $d\Lambda/d\varepsilon \neq 0$ at $\varepsilon = 0$).

The eigenfunction corresponding to μ_{01}, the lowest eigenvalue for $m = 1$, is

$$\phi_0 = \chi_{01}(r)\cos(2\pi z/L). \tag{24}$$

According to (23), $\kappa_0 = 0$ for solutions branching from μ_{01}, since the defining integrals extend over one period in z and the numerator therefore vanishes. The differential equation determining ϕ_1, from (20b), is now

$$L(0,\mu)\phi_1 = -\left[\mu_{01}p_2(r) - r^{-2}q_2(r)\right]\phi_0^2 \qquad (25)$$

$$= -\frac{1}{2}\left[\mu_{01}p_2(r) - r^{-2}q_2(r)\right]\left[1 + \cos\frac{4\pi z}{L}\right]\chi_{01},$$

with solutions in the form

$$\phi_1 = f_1(r) + f_2(r)\cos\frac{4\pi z}{L}. \qquad (26)$$

The direction of the bifurcation is fixed now by κ_1. Assuming $\kappa_1 \neq 0$, $\Lambda(\varepsilon) - \mu_{01} = \kappa_1\varepsilon^2 + \ldots$, and the bifurcation there is a pitchfork ($\frac{d\Lambda}{d\varepsilon} = 0$ and $\frac{d^2\Lambda}{d^2\varepsilon} \neq 0$ at $\varepsilon = 0$). The value of κ_1 is determined by the solvability of (20c), and the formula corresponding to (23) is,

$$\kappa_1 = -\frac{\langle 2s_2(r;\mu)\phi_0^2\phi_1 + s_3(r;\mu)\phi_0^4\rangle}{\langle p_1(r)\phi_0^2\rangle}, \qquad (27)$$

and this does not generally vanish.

The solutions bifurcating at μ_{01} are wavetrains with wavelength L in an axially infinite region. By developing the series solution in ε, a finite amplitude periodic wavetrain may be constructed.

When $L \to \infty$, $\mu_{01} = \mu_{00} + O(L^{-2})$, and the solution of the inhomogeneous ordinary differential equation for $f_1(r)$ is of $O(L^2)$. As a consequence, the series (18a) becomes disordered when $\varepsilon L^2 = O(1)$. The way to deal with this non-uniform behavior for long-waves by the method of multiple scales (or equivalent methods) is well-known. In the context of the approach taken here, the expansion is centered about the columnar bifurcation point, μ_{00}. The procedure, sketched in Leibovich (1987), goes as follows. Letting Z be the slow scale, with $Z = z\sqrt{\varepsilon}$, $\Phi = A(Z)\phi_0(r)$ (at lowest order), then $\phi_0(r)$ is the principal eigenfunction corresponding to the eigenvalue μ_{00}, and A satisfies the equation

$$\frac{d^2A}{dZ^2} + \alpha A^2 + \beta\kappa_0 A = 0 \qquad (28a)$$

where κ_0 is defined by (18b), as before, but is no longer restricted by the solvability condition (23), and

$$\alpha = \frac{\langle s_2 \phi_0^3 \rangle}{\langle \phi_0^2 \rangle} \quad , \quad \beta = \frac{\langle p_1 \phi_0^2 \rangle}{\langle \phi_0^2 \rangle} \tag{28b}$$

The analysis, although by a different route, is essentially that of Benjamin (1967).

Equation (28a) has the solitary wave solution

$$A = a \operatorname{sech}^2 [\sqrt{a\alpha/6}\, Z] = a \operatorname{sech}^2 [\sqrt{a\varepsilon\alpha/6}\, z] \tag{29a}$$

provided $a\alpha > 0$ (and has no such solution otherwise). The constant a in (29) is related to the parameters in (28a); with the level of the extreme value of A set to be a and placed at $z = 0$, as has been done in (29), the amplitude a, or more precisely, εa, is linearly related to the swirl rate by

$$\Lambda = \mu_{00} - \frac{2\alpha}{3\beta} \varepsilon a. \tag{29b}$$

In this discussion, it has been assumed that ε is positive, so that waves of elevation or depression depend on whether a is positive or negative: since we must have $a\alpha > 0$, the question devolves to the sign of α, which is a functional of the specifying flow. Furthermore, since $\beta > 0$, (29b) shows that solitary waves may exist only for $\Lambda < \mu_{00}$. In this parameter regime, no standing waves are possible (since they all branch from eigenvalues greater than μ_{00}), and by definition this is a supercritical regime. Thus (29b) makes clear that weakly nonlinear solitary waves form only on supercritical flows. Further discussion of the criticality classification is given in §5.1.

The weakly-nonlinear solitary wave solutions found by Leibovich (1970) from the time-dependent Korteweg-deVries equation are equivalent to those given above. This alternative form effectively derives from the alternative parameterization of the time-independent problem by wave speed (instead of swirl level) mentioned in the Introduction and is

$$\Phi = \varepsilon a\, \phi_0(r) \operatorname{sech}^2 \left[\frac{1}{2} \left(\frac{c_1 a}{3 c_2} \right)^{\frac{1}{2}} (z - c_0 t + \tfrac{1}{3} \varepsilon a c_1 t) \right] \tag{30}$$

where a is an arbitrary amplitude, ϕ_0 is the eigenfunction of the linearized problem equivalent to (27), the c_i are constants depending on the base flow and ϕ_0, and are equivalent to α and β in (28). For a given base flow, the value of εa determines the wave amplitude and therefore its velocity; or, alternatively, the change in the base flow axial component that would make the solution stationary. Changing λ (that is, the azimuthal component) instead will produce the same results provided the swirl ratio is the same; so

selecting an eigenvalue and setting λ (or Λ) completely determines this approximate solution.

The numerical construction of solutions along a branch can be done by a simple continuation method, starting with solutions generated numerically by the perturbation procedure described above.

3.3. Branch continuation

To "continue" (Kubicek & Marek, 1983, gives a good summary of continuation and bifurcation methods) a solution (Φ_0,Λ_0) known at a given value of $\Lambda = \Lambda_0$, to a neighboring value differing from Λ_0 incrementally, we could proceed by taking Φ_0 as an initial guess for $\Phi(\Lambda_0 + \Delta\Lambda)$ in a suitable iterative procedure, such as Newton's method,

$$\Phi_{n+1} = \Phi_n - L^{-1}(\Phi_n,\Lambda)N(\Phi_n,\Lambda) \tag{31}$$

using an appropriate discretization for L and N. This will give a solution if L is not singular, that is, if no bifurcation or turning point is encountered, and if $\Delta\Lambda$ is sufficiently small. To increase the size of $\Delta\Lambda$ while still providing a good guess for the iteration, we can proceed in the following standard way by differentiating along solution arcs $(\Phi(\Lambda),\Lambda)$: since

$$N(\Phi(\Lambda),\Lambda) = 0,$$

$$\frac{dN}{d\Lambda}(\Phi,\Lambda) = \frac{\partial N}{\partial \Phi}\Big|_{\Phi;\Lambda} \cdot \frac{\partial \Phi}{\partial \Lambda} + \frac{\partial N}{\partial \Lambda}\Big|_{\Phi;\Lambda} = 0. \tag{32a}$$

Then, at any point (Φ,Λ), the "slope" of the solution curve

$$\dot{\Phi} \equiv \frac{\partial \Phi}{\partial \Lambda} = -\left(\frac{\partial N}{\partial \Phi}\Big|_{\Phi;\Lambda}\right)^{-1} P(\Phi) = -L^{-1}(\Phi,\Lambda)P(\Phi) \tag{32b}$$

assuming the linearized operator $L(\Phi,\Lambda)$ is invertible with inverse $L^{-1}(\Phi,\Lambda)$. We can think of (31) as a differential equation for Φ as a function of Λ. We use (31) and (32b), in a numerical algorithm described in the appendix, in a predictor-corrector mode. We first integrate (32), using a Runge-Kutta method to arrive at an estimate for Φ at $\Lambda_0 + \Delta\Lambda$ assuming a solution is known at Λ_0, and then refine this estimate using Newton iteration (31). We begin each solution branch by using a three-term perturbation expansion, also described in the appendix, which is the discrete version of the analysis given in §3.2. This

procedure will fail if secondary bifurcation points or turning points are encountered as a given branch is traced, and then a more involved procedure, such as that devised by Keller (1977) (see also Kubicek & Marek, 1983) will be required. We did not encounter such complications in the course of our investigations.

To do detailed calculations, we must select a particular specifying flow. We will explore the possible branches of solutions stemming from the following simple columnar vortex, which has been previously treated by Leibovich (1970):

$$W(r) = 1 \tag{33}$$

$$V(r) = \frac{\lambda}{r}\{1 - \exp(-\alpha r^2)\}.$$

This example is known as the Burgers-Rott vortex. It corresponds to the following specifications of the functions arising in §2:

$$\Psi(r) = \frac{1}{2}r^2, \quad R(\psi) = 2\sqrt{\psi}, \quad f(\psi) = 1 - \exp(-2\alpha\psi) \tag{34}$$

$$A(\psi) = 0; \quad B(\psi, r^2) = (\psi - \frac{1}{2}r^2)\, 2\alpha \exp(-2\alpha\psi)\{\frac{1 - \exp(-2\alpha\psi)}{\psi}\},$$

$$P(\Phi) = B(\frac{1}{2}r^2 + \Phi, r^2) - B(\frac{1}{2}r^2, r^2); \quad Q(\Phi) = 0.$$

3.4 Numerical Implementation

The problem stated in (16) is discretized using central differences on a rectangular mesh in the meridional plane (r,z). Let $\underline{\Phi}$, $\underline{D}$, $\underline{\Omega}$ be the finite-dimensional counterparts of Φ, D^2, Ω, as defined in the appendix; (16) then corresponds to the matrix equation—

$$\underline{D}\,\underline{\Phi} + \underline{\Omega}(\underline{\Phi}, \Lambda) = 0 \tag{35}$$

Equation (35) is the basis for the numerical treatment. We do not discretize steps of the analytical procedure separately; rather, we provide an equivalent analysis for the approximate equation (35). A separate discretization of (22), for example, leads to eigenvalues that are slightly different than the bifurcation points of (35), and this is enough to prevent convergence to a solution branch in some cases. Even more telling, if eigenvectors obtained from the algebraic eigenvalue problem are used in conjunction with a semianalytic enforcement of an orthogonality condition (for example, by means of a numerical quadrature), then the result will not be precisely orthogonal in the algebraic problem, and if the next stage of the problem is solved algebraically, errors are introduced. We therefore re-derive equations (17)–(29) in the appendix for the algebraic system (35). This ensures consistency of numerical values throughout the analysis.

The strategy is the same as that described in §§3.2 and 3.3. First, a solution point on a non-trivial branch is sought using a perturbation expansion (or, for the solitary wave branch, the weakly-nonlinear solution may be used). Numerical integration of the discrete analog of (32b) continues the branch away from the bifurcation point, and Newton's iterations serve as corrector steps at selected points along the branch.

4. Columnar-columnar bifurcations and continuation

In this section, we discuss some general questions about bifurcations of the specifying columnar flow to other columnar flows, and then give numerical results for the example specified in (34).

4.1. Transfer of B-criticality condition

Benjamin (1962) has provided a simple test to determine whether a given columnar vortex is subcritical or supercritical. As Leibovich (1979) has shown, this turns out to be an appropriate test (for axisymmetric disturbances) even though the crucial quantity determining whether upstream propagation of disturbances is possible is the group, not the phase, speed. Subcritical flows can be expected to be influenced by small downstream disturbances. This might be true even in flows that are supercritical according to this classification scheme, since it does not cover nonaxially symmetric perturbations, but the propagation characteristics of nonaxially symmetric waves (see Leibovich et al., 1986) is more difficult to determine. Benjamin's criticality classification is important because it seems to be useful in correlating vortex breakdown data (Leibovich, 1983, 1984), as Squire (1960) and Benjamin (1962) had proposed. In particular, the evidence (see Leibovich, 1978, or *L*) indicates that flows upstream of vortex breakdowns are supercritical, while the (mean) flows downstream are subcritical.

To determine the criticality condition of a given columnar flow, we ask whether it can sustain infinitesimal waves of the form

$$o = \chi(r)\, e^{ikz}, \tag{36}$$

which means that equation (16a) has a solution in the form

$$\Phi + \varepsilon o$$

for infinitesimal ε. This leads to a problem similar to that in §3.1, except that we wish to consider columnar flows other than the specifying flow (which has $\Phi = 0$), and, rather than fixing the wavelength (= L) and searching for values of Λ for which the linearized problem is solvable, the question is turned around: Λ is fixed, and we ask if there is any real value of k (= $2\pi/L$) for which the linearized problem is solvable. If so, a standing wave with wavenumber k determined is possible and the flow is subcritical. If not, the flow is supercritical. Let

$$\hat{L}(\Phi,\Lambda)(\ ) = \frac{\partial^2(\ )}{\partial r^2} - \frac{1}{r}\frac{\partial(\ )}{\partial r} + \left[\Lambda\frac{\partial P}{\partial \Phi}(\Phi,r) - r^2\frac{\partial Q}{\partial \Phi}(\Phi,r)\right](\ ) \tag{37}$$

then we may write the differential equation for the small wavy perturbations as

$$-\frac{\partial^2 o}{\partial z^2} = k^2 o = \hat{L}(\Phi,\Lambda)\, o. \tag{38}$$

We now regard this as an eigenvalue problem for k^2, with Λ fixed. It is, due to (36), an ordinary differential equation for χ in standard Sturm-Liouville form and subject to the boundary conditions $\chi(a) = \chi(1) = 0$.

We know that the specifying flow is supercritical for $\Lambda < \mu_{(0)}$ (because there are no eigenvalues of (17) in this range of Λ, either corresponding to columnar flows or to wavy flows, according to §3.1), and subcritical for $\Lambda > \mu_{(0)}$, because, according to the observation of §3.1, there is a wave with *some* wavenumber for each value of $\Lambda > \mu_{(0)}$, with waves with indefinitely long wavelengths branching off indefinitely close to $\mu_{(0)}$. If $\Lambda = \mu_{(0)}$, it is clear that the eigenvalue k^2 of (38) vanishes, and we may summarize by observing that the eigenvalue k^2 of (38) is negative if $\Lambda < \mu_{(0)}$, zero for $\Lambda = \mu_{(0)}$, and positive for $\Lambda > \mu_{(0)}$, and that

$$\frac{dk^2}{d\Lambda} > 0 \text{ at } \Lambda = \mu_{(0)}.$$

We wish to characterize the criticality condition of the columnar vortex branching off from the specifying flow at $\Lambda = \mu_{(0)}$, on either side of the bifurcation point. To explore this, we differentiate (38) with respect to Λ, to arrive at an inhomogeneous equation for $\frac{\partial \chi}{\partial \Lambda}$

$$\hat{L}(\Phi,\Lambda)\frac{\partial \chi}{\partial \Lambda} - k^2\frac{\partial \chi}{\partial \Lambda} = \frac{dk^2}{d\Lambda}\chi - \frac{d\hat{L}(\Phi,\Lambda)}{d\Lambda}\chi, \tag{39a}$$

where,

$$\frac{d\hat{L}(\Phi,\Lambda)}{d\Lambda}\chi = \frac{\partial\Phi}{\partial\Lambda}\left[\Lambda\frac{\partial^2 P}{\partial\Phi^2}(\Phi,r) - r^2\frac{\partial^2 Q}{\partial\Phi^2}(\Phi,r)\right]\chi + \frac{\partial P}{\partial\Phi}(\Phi,r)\chi. \tag{39b}$$

Since χ satisfies (38), (39) is solvable only if

$$\frac{dk^2}{d\Lambda} = \frac{\langle \chi \frac{d\hat{L}(\Phi,\Lambda)}{d\Lambda} \chi \rangle}{\langle \chi^2 \rangle} \tag{40}$$

We are interested in (40) at $\Lambda = \mu_{(0)}$, $\Phi = 0$. The numerator of (40) is

$$\langle \chi^2 \{ 2s_2(r,\mu)\dot{\Phi} + p_1(r) \} \rangle \tag{41}$$

where we have used the notation of (21) and (32b). The only difference in (40), when evaluated at the bifurcation point for either of the intersecting solution curves is the direction, $\dot{\Phi}$, of the particular solution curve along which $\frac{dk^2}{d\Lambda}$ is evaluated. On the specifying flow, $\frac{\partial\Phi}{\partial\Lambda} = 0$, and on the second branch $\dot{\Phi} = \chi$, the eigenfunction, apart from an arbitrary multiplicative constant which we take to be unity. Thus, along the specifying flow, (40) reduces to

$$\frac{dk^2}{d\Lambda} = \frac{\langle p_1(r)\chi^2 \rangle}{\langle \chi^2 \rangle} \tag{42}$$

To calculate the numerator of (40) for the nontrivial bifurcating solution, we differentiate (32a) twice with respect to Λ. The result, when evaluated at $\Phi = 0$, $\Lambda = \mu_1$, is

$$\hat{L}(0,\mu_{(1)})\ddot{\Phi} + 2\mu_{(1)}s_2(r,\mu_{(1)})\dot{\Phi}^2 + 2p_1(r)\dot{\Phi} = 0,$$

and solvability for $\ddot{\Phi}$ requires

$$\dot{\Phi}^2 \{ 2s_2(r,\mu_{(1)})\dot{\Phi} + 2p_1(r) \} \rangle = 0. \tag{43}$$

Combining (43) with (41), we find that on the bifurcating branch,

$$\frac{dk^2}{d\Lambda} = -\frac{p_1(r)\dot{\Phi}^2}{\dot{\Phi}^2} = -\frac{\langle p_1(r)\chi^2 \rangle}{\langle \chi^2 \rangle} \tag{44}$$

which is just the negative of (42). Therefore, since $\tilde{k}^2$ increases through zero as Λ increases through $\mu_{(0)}$ on the specifying flow branch, is must decrease through zero as Λ increases through $\mu_{(0)}$ on the principal branching solution.

Thus, we have shown that the criticality conditions holding on the specifying flow and that holding on the flow branching transcritically from it are transferred at the bifurcation point: this will be illustrated in §4.3. If we hold Λ fixed, our problem conforms to that considered by Benjamin (1962), who labels each columnar flow distinct from the specifying flow - and there may be more than one depending on the value of Λ - as 'conjugate' to the specifying flow. Benjamin shows that, if the primary flow is supercritical, then *all* conjugate flows must be subcritical. This is consistent with the local results of this section.

4.2. Stability is not transferred

Stability of the steady solutions treated here cannot be addressed using the BHE, since it contains no dynamics. Instead, one must return to the Euler equations. As a rule, vortex flows tend to less stable to nonaxisymmetric perturbations than to axially symmetric ones. A bifurcation point is usually associated with a transfer of stability, so that in the present case, one would suppose that the specifying flow is stable and the principal branch is unstable on one side of the bifurcation point $\Lambda = \mu_{(0)}$, with the reverse being the case on the other side. This is assured if the eigenvalues of the temporal linearized stability problem, deriving from the Euler equations, are simple, and provided they move with a nonzero speed across the imaginary axis. In our example (33), at least when strictly restricted to axisymmetric disturbances, the temporal eigenvalues are simple at the bifurcation points of the BHE equation, but bifurcation need not be associated with loss of stability, which implies that the temporal eigenvalues in such cases are confined to the imaginary axis. This may be seen from the axially-symmetric Howard-Gupta equation (Howard & Gupta, 1962), which governs the temporal stability problem. This equation is identical to (17a) provided only that the axial velocity of the specifying flow, $W(r)$, be replaced by $W(r) - c$, where $c = \frac{\omega}{k}$ is the (in general complex) phase speed, and $\sigma = i\omega$ is the temporal eigenvalue. In the example vortex (33), bifurcation does not lead to loss of stability. Here the Rayleigh discriminant is positive and there is no axial shear. Therefore, by Rayleigh's (1882) stability criterion, (33) is linearly stable to axisymmetric perturbations for all Λ. On the other hand, the same stability condition must hold for the solution branching from this point, at least for a limited range of Λ. This must be so since the linearized stability characteristics there are determined by the unperturbed flow at the bifurcation point, which is the same for all branches meeting there. Because the velocity profiles on the bifurcating branch deform continuously with Λ, there will be a finite Λ interval over which the Richardson number criterion of Howard and Gupta, which generalizes Rayleigh's criterion to admit axial shear, continues to guarantee linear stability to axially-symmetric perturbations. The eigenvalues, σ, of the temporal stability problem

can be found from the eigenvalues, μ, of the static bifurcation problem in the primary flow selected for numerical treatment (for which $W(r) = 1$), since it is easy to show that

$$\sigma = ik\left(1 \pm \frac{\Lambda}{\mu}\right).$$

The eigenvalues σ are simple and lie on the imaginary axis for all Λ, and the zero eigenvalue is assumed when $\Lambda = \mu$.

Szeri (1988) has shown that, within the confines of the Arnold-Casimir theory, these results may be extended to weakly nonlinear stability. (The interpretation of this theory and its significance, as applied to this problem, is a complicated matter that requires and deserves further study.)

4.3. Numerical results

Figure 1 is bifurcation diagram for the columnar solutions branching from the primary flow (33,34) with $\alpha = 1.4$, showing the principal and the second bifurcating branches. (The locations of the points of bifurcation are given in Table 1 in §5.) The branches are described by a measure of the perturbation axial velocity. We took this to be the extreme value (regardless of sign), and on the principal bifurcating branch, on which the perturbation axial velocity is monotonic in r, this always occured at the axis of rotation. On the second branch, the perturbation axial velocity if not monotonic. On this branch, a discontinuity appeared in the bifurcation diagram based upon this measure described: for a range of swirl parameter, the extreme value occured on the axis, but shifted to a point off the axis, where the perturbation axial velocity was of opposite sign. This is illustrated by two sets of points in the figure, one as described, and the other (smooth) set arrived at by plotting only the perturbation axial velocity on the axis.

(FIGURE 1 ABOUT HERE)

The principal columnar branch plays an important role, as will be seen. In contrast, the physical significance of the second and higher columnar branches is unclear - for the larger amplitude perturbations on these branches, axial flow reversals are necessarily accompanied by internal zeros of the swirl, and hence instability according to the Rayleigh-Synge (1933) criterion (abbreviated subsequently by R-S). This may be seen in figure 2, which shows profiles from three points on the second branch of figure 1. Here the bifurcation point occurs at $\Lambda = \mu_{10}$, and the profiles are drawn for increasing values of Λ/μ_{10}. One can also see from the profiles for axial velocity how the discontinuity in the bifurcation diagram discussed in the previous paragraph arises. We will not further discuss columnar branches other than the principal branch.

(FIGURE 2 ABOUT HERE)

For $\Lambda < \mu_{(0)}$, the principal branch shows a developing wake-like axial velocity profile as the swirl parameter Λ is decreased from the branch point $\mu_{(0)}$, as may be seen in figure 3. The swirl velocity is distorted as well, with the peak swirl moving outwards relative to that in the primary vortex. Both of these characteristics are qualitatively like the time-averaged profiles measured by Garg and Leibovich (1979) (further analysis of this data is given by *L* and by Leibovich, 1978) *downstream* of vortex breakdowns, which are, like the solutions here, wake-like and subcritical. If the Λ/μ_{00} is decreased below a value of about 0.5, the swirl velocity develops an internal zero, and the branch will become unstable according to the R-S criterion. We have nevertheless continued to

(FIGURE 3 ABOUT HERE)

follow the branch, being curious to know if it could be continued to zero swirl, or whether it would turn around. We found that it *can* be continued to zero swirl, and the curvature of the magnified part of the bifurcation diagram of figure 1 indicates that the axial speeds get large as $\Lambda/\mu_{00} \to 0$. The axial profiles shown for $\Lambda/\mu_{00} = 0.001$ suggest that the limit flow becomes discontinuous, with a vortex sheet forming in the interior. The resolution of the singular limit behavior as $\Lambda/\mu_{00} \to 0$ requires special treatment, and §4.4 is devoted to this question.

On the $\Lambda/\mu_{00} > 1$ side of the principal branch, the axial velocity profiles are jet-like, and the peak swirl moves towards the axis relative to that in the primary vortex. Examples are shown in figure 4. No tendency towards R-S instability occurs on this side of the bifurcation point. These

(FIGURE 4 ABOUT HERE)

velocity profiles not only resemble the profiles measured by Faler and Leibovich (1977,8) and in the references cited in the previous paragraph for flows well *upstream* of vortex breakdown, they also can be accurately fitted, as can the wake-like solutions previously discussed, by the same exponential functions used in those references. We note further that the experimental data shows the upstream flow to be not only jet-like, but supercritical. Thus, the primary vortex with *uniform* axial velocity generates, through its principal branch, vortices of the same character as those found on *both* upstream and downstream sides of experimentally observed vortex breakdowns, so far as the shapes of the profiles and their criticality conditions are concerned.

For $\Lambda < \mu_{(0)}$, the primary vortex is supercritical and the principal branch is subcritical, and according to the general theory of §4.1, these characteristics should be exchanged when $\Lambda > \mu_{(0)}$. We have tested this by computing the generalized Froude number, N, proposed by Benjamin (1962). This is defined to be

$$N \equiv \frac{c_+ + c_-}{c_+ - c_-}.$$

where c_+ and c_- are, respectively, the maximum and minimum phase speeds of infinitesimal axisymmetric waves of extreme length propagating on the vortex. If $N > 1$, a vortex is supercritical, and if $N < 1$ it is subcritical. We have computed N on both the primary vortex and the principal branch, and the results, given in figure 5, confirm the general theory on exchange of criticality at the bifurcation point.

(FIGURE 5 ABOUT HERE)

4.4. Singular limit of zero swirl

For the specifying flow (34) that we have been using as example, the zero swirl limit $\Lambda=0$ is irrotational, and the constant speed flow $\psi = \frac{1}{2} r^2$ is unique. Therefore no differentiable solutions exist except for the specifying flow. On the other hand, our numerical results suggest that the limit $\Lambda \to 0+$ along the principal columnar branch develops a strong shear layer tending in the limit to a vortex sheet separating two piecewise irrotational *limiting flows, in each section of which* the flow is oppositely directed and of uniform infinite speed! We explore this bizarre situation by an asymptotic development that seems to fit with the numerical findings, and which gives the asymptotic dependence of the velocity levels, and of the shear layer location and thickness on Λ.

It is convenient here to work with the total streamfunction ψ, governed by (11), rather than the perturbation from the specifying flow. For the specifying flow (34), the limit of equation (11) when $\Lambda=0$ is $D^2\psi = 0$, with a solution that is linear in r^2. We assume the existence of a discontinuity in this limit, located at $r=r_*$, at which the streamfunction reaches its minimum value, $\psi(r_*) \equiv -\psi_*(\Lambda)$. The analysis of this section in simplified by the change of variable

$$\eta = \frac{1}{2} r^2.$$

Then we may write (using the condition that $\psi = 0$ at $\eta = 0$ and $\psi = \frac{1}{2}$ at $\eta = \frac{1}{2}$, and defining $\eta_* = \frac{1}{2} r_*^2$)

$$\begin{aligned} &\psi = C\,\eta, \text{ for } \eta - \eta_* < 0 \\ &\psi = D\,(\eta - \tfrac{1}{2}) + \tfrac{1}{2}, \text{ for } \eta - \eta_* > 0. \end{aligned} \tag{45}$$

For Λ very small but not zero, we assume the existence of a single internal layer, centered on η_* and with a thickness $\delta(\Lambda)$ that tends to zero as $\Lambda \to 0+$, that joins these two constant speed solutions. Furthermore, the numerical results suggest that $\psi_*(\Lambda) \to \infty$ as $\Lambda \to 0$, and we also assume this.

The solution to the outer problem has been described above, and now we seek a structure to the internal boundary layer separating the two irrotational regions. It is important (and easy to show) that $D^2\psi = 0$ to *all* algebraic orders in the small parameter in the outer regions, so that the full outer expansions retain the form (45), with the coefficients of η being functions of Λ. The point η_*, and the constants C and D occuring in the outer problem are not yet known and must be determined by matching with this internal boundary layer. The argument is reminiscent of activation energy asymptotics (see Buckmaster and Ludford, 1982). Stretch the radial scale near $\eta = \eta_*$, by taking

$$\eta \equiv \eta_* + \delta X = \eta_*(1 + \mu X), \quad \mu \equiv \frac{\delta}{\eta_*} \tag{46}$$

where δ is the length scale appropriate in the layer and it is assumed that $\delta(\Lambda) \to 0$ as $\Lambda \to 0$. Near η_* the streamfunction is continuous and the appropriate scale for it is $\psi_*(\Lambda)$, so we write

$$\psi(\eta_* + \delta X) = -\psi_*(\Lambda)[1 + \varepsilon(\Lambda)\, y(X;\Lambda)] \tag{47}$$

in the layer, where the asymptotically small parameter $\varepsilon(\Lambda)$, like the parameters $\delta(\Lambda)$, and $\psi_*(\Lambda)$, remain to be identified. From the definition of $-\psi_*(\Lambda)$ as the extreme value of ψ, we must have

$$y(0;\Lambda) = y'(0;\Lambda) = 0 \tag{48}$$

where $(\,)' \equiv \frac{d}{dX}$, and we also have $y \le 0$ for all X. We substitute the ansatz (45-47) into (11) and invoke (34). This yields

$$y'' + \frac{2\alpha\Lambda\delta^2}{\varepsilon\psi_*} f(y) = 0$$

where

$$G(y) \equiv \left(\frac{1}{2\eta} - \frac{1}{2\psi_*(1-\varepsilon y)}\right) e^{-4\alpha\psi_*(1+\varepsilon y)}\left(1 - e^{-2\alpha\psi_*(1+\varepsilon y)}\right).$$

The distinguished limit arises for $2\alpha\psi_*\,\varepsilon$ and $2\alpha\Lambda\delta^2 e^{-4\alpha\psi_*}/2\eta_*$ both O(1), and we therefore set

$$2\alpha\psi_*\,\varepsilon = 4\alpha^2\Lambda\delta^2 e^{-4\alpha\psi_*}/2\eta_* = 1. \tag{49}$$

which leads to the equation

$$y'' + \left[\frac{1}{1+\mu X} + \frac{2\eta_*\alpha\varepsilon}{1+\varepsilon y}\right]e^{2y} = 0, \tag{50}$$

with exponentially small error. We may now look for a solution to this inner problem in the form of power series in the small parameter. It is more convenient in the analysis to regard ε as the controlling small parameter rather than Λ, and so we take

$$y = y_0 + \varepsilon y_1 + \ldots \tag{51}$$

$$\mu = \mu_1\varepsilon + \mu_2\varepsilon^2 + \ldots \tag{52}$$

$$\frac{1}{2\eta_*} = \gamma_0 + \gamma_1\varepsilon + \ldots \tag{53}$$

and the slightly unconventional form of the last expansion makes the matching with the outer solution simpler.

The equations for first two coefficients, y_0 and y_1, of (51) are

$$y_0'' + e^{2y_0} = 0 \tag{54}$$

$$y_1'' + 2e^{2y_0}y_1 = \left[\mu_1 X - \frac{\alpha}{\gamma_0}\right]e^{2y_0}. \tag{55}$$

The solution to (54) satisfying (48) is

$$y_0(X) = \ln \operatorname{sech}(X), \tag{56}$$

and the solution to (55) is

$$y_1(X) = \frac{1}{2}\left[\mu_1(X - \tanh X) - \frac{\alpha}{\gamma_0} X\tanh X\right]. \tag{57}$$

We now match the streamfunction in the inner region with the two outer regions. Matching to second order in ε yields

$$\frac{1}{2\eta_*} = (2 + \varepsilon(1+\alpha)) + \gamma_2\varepsilon^2 ; \tag{58a}$$

$$C = -\frac{1}{2\alpha\varepsilon\eta_*}(1 + \varepsilon \ln 2 + \frac{1}{2}\varepsilon^2) \tag{58b}$$

$$D = -\frac{1}{2\alpha\varepsilon\eta_*}(-1 + \varepsilon(1 - \ln 2) + \varepsilon^2 b_2) \tag{58c}$$

$$\mu = \varepsilon + \varepsilon^2(\frac{1}{2} + \frac{1}{4}\alpha - \ln 2) \tag{58d}$$

$$\delta = \eta_*\mu, \tag{58e}$$

and from these we can find

$$\Lambda = 2\eta_*(2\alpha\delta \exp(2\alpha/\varepsilon))^{-2}. \tag{58f}$$

The numbers γ_2 in (58a) and b_2 in (58c) are undetermined at this order, and therefore our solution is completely determined only to one order less than we have shown - on the other hand, it is necessary to match at the level shown to accurately determine the solution to that order (i.e., to within an error of $O(\varepsilon)$).

The composite expansion for ψ constructed from (45-47,56-58) is

$$\begin{aligned}\psi = &-\frac{1}{2\alpha\varepsilon}\Big\{(1 + \varepsilon \ln 2)\frac{\eta}{\eta_*}H(\eta_* - \eta) \\ &+ (-1 + \varepsilon(1 - \ln 2 + \frac{\eta - \frac{1}{2}}{\eta_*})H(\eta - \eta_*) \\ &+ \varepsilon\Big[\ln\tfrac{1}{2}\operatorname{sech}\Big(\frac{\eta - \eta_*}{\delta}\Big) + \Big|\frac{\eta - \eta_*}{\delta}\Big|\Big]\Big\} \\ &+ \tfrac{1}{2}H(\eta - \eta_*); \quad \psi(r_*) = -\frac{1}{2\alpha\varepsilon}.\end{aligned} \tag{59}$$

where $H(t)$ is the unit function, $H(t) = 1$ for $t > 0$, $H(0) = \frac{1}{2}$, and $H(t) = 0$ for $t < 0$.

Equations (58) give $\hat{o}$, r_*, and Λ as a function of the parameter ε, and from them the dependence of $\hat{o}$ and r_* on Λ can be evaluated to yield the desired asymptotic relationship between these parameters as $\Lambda \to 0$. As seen in figure 6, the differences between the computed and the asymptotic values are only a few percent for $\Lambda = 0.01$. The asymptotic solution (59) is compared in figure 7 to the computed streamfunction and axial velocity for $\Lambda = 1.769 \cdot 10^{-4}$. The agreement is quite good, considering the fact that $\psi_* = 0.13$, not yet large as the analysis assumes, meaning that the asymptotic relation is good far beyond its expected region of $|\psi_*| >> 1$.

(FIGURES 6 & 7 ABOUT HERE)

The azimuthal velocity component, v, is exponentially small except in the shear layer. The shear layer is a concentrated region of vorticity, with both axial vorticity arising from the swirl as well as azimuthal vorticity arising from the variation in axial velocity across the layer present. As $\Lambda \to 0$, the swirl component $v \to 0$ in the layer as $\sqrt{\Lambda}/|\ln \Lambda|$, which is very much slower than Λ.

5. Periodic wavetrains

The specifying flow is subcritical for $\Lambda > \mu_{00}$: for any Λ in this range, an infinitesimal standing wave is possible, with wavelength depending on Λ. Fixing the wavelength at L, we continue infinitesimal standing waves to finite amplitude for the specifying flow (34) with $\alpha = 2$ and $\alpha = 14$ using the methods previously described. The larger value of α was used in an earlier study by Leibovich (1970), because it provided a good fit to Harvey's (1962) experimental data. The eigenvalues μ_{pm}, determined numerically as described in the Appendix, are given in Table 1 for $\alpha = 2$ for $L = 6$ and 20, and for $\alpha = 14$ for $L = 6, 20, 100$.

α	L	μ_{00}	μ_{01}	μ_{10}
2	6	1.8433	1.9693	6.2743
	20	1.8433	1.8547	6.2743
14	6	.17390	.17986	.61147
	20	.17390	.17445	.61147
	100	.17390	.17392	.61147

Table 1. Eigenvalues of the linearized problem for selected values of L and α.

Figure 8 is the bifurcation diagram for the case $\alpha = 2$ and $L = 10$. The diagram for $\alpha = 14$ is qualitatively similar, but the separation between the curves for the columnar branch and the first wavy branch closes too rapidly to be conveniently illustrated in a drawing. The solid line gives the columnar (00) branch, open circles the fundamental wavy branch (01), and the close circles the first harmonic wavy branch (02).

(FIGURE 8 ABOUT HERE)

We next explore the waveform for three flows on the fundamental wavy branch for the case $\alpha = 14$, $L=10$. The streamfunction at a fixed value of $r = 0.25$ is plotted in figure 9 as a function of z over one wavelength , for three values of Λ/μ_{00}. As Λ/μ_{00} increases, the wave trough becomes increasingly sharp and concentrated, and the wave crests increasingly broad and flat. The same trend is seen if the fundamental wavy branches for a sequence of flows of increasing wavelength L are sampled at fixed Λ/μ_{00}.

(FIGURE 9 ABOUT HERE)

Figure 10 shows streamlines projected onto a meridian plane for increasing values of Λ/μ_{00} for the case $L = 6$ and $\alpha = 14$. The deceleration of the upstream flow caused by the wave is apparent at the smallest value of Λ/μ_{00} shown. The other two streamline fields reveal a region of closed streamlines, with the size of the recirculation region growing with Λ/μ_{00}.

(FIGURE 10 ABOUT HERE)

The changes in waveforms as either $(\Lambda - \mu_{00})/\mu_{00}$ or L increases are illustrated in figure 9. Increases in either of these parameters appear to produce a wave shape with a very sharp trough, in which there are strong axial accelerations, rapidly tending to a broad flat crest. Over most of its extent, this broad crest is an essentially columnar flow, but distorted considerably from the primary columnar flow. These features are characteristic of a solitary wave, with $L = \infty$, on a columnar flow different from the specifying flow.

Velocity profiles at the wave trough are given in figure 11a,b for a two swirl levels large enough to cause a region of reversed axial flow to appear. Figure 11c shows the difference between the axial velocity at the trough and the axial velocity at the crest, where the flow is nearly columnar and, as will be shown, virtually indistinguishable from the principal conjugate flow. This is a perturbation caused *to the principle conjugate flow* by the disturbance concentrated near the wave trough, rather than a perturbation to the specifying flow. The profiles in 12c are similar to the perturbation axial velocity in solitary waves on the specifying flow.

(FIGURE 11 ABOUT HERE)

The observations we have made about the apparent appearance of solitary wave behavior will now be put to quantitative tests.

The characteristic length of a solitary wave can be measured by, say, its half-height length. According to the weakly nonlinear soliton solution (29), the half-height length (or any other measure of the solitary wave length) scales with the inverse square root of the wave amplitude, $1/\sqrt{\varepsilon a}$, or alternatively, with $1/\sqrt{|\Lambda-\mu_{00}|}$, at least for $|\Lambda - \mu_{00}|$ sufficiently small. The axial velocity perturbation at the origin is proportional to the wave amplitude, εa. In figure 12 we have plotted the half-height calculated from our numerically determined solutions on the first wavy branch for several wavelengths L = (6,20,100), against the axial velocity perturbation at the origin to test to see whether the amplitude-length scaling appropriate to the weakly nonlinear solitary wave is approached by a wave of the computed periodic wavetrain. Waves exhibiting that scaling will have a slope of $-\frac{1}{2}$ on this log-log plot, and the solid line drawn has that slope. The wavetrain with period L = 6, given by the open circles, deviates substantially from the $-\frac{1}{2}$ slope both for small and large wave amplitude. The longer waves, however, accurately display the solitary wave scaling for amplitudes ranging from fairly small values to quite substantial ones. Marked deviations from the weakly nonlinear solitary wave scaling occur for for very small axial velocity perturbations and for axial velocity perturbations of O(1) and higher. As will be seen in the next section, strong nonlinear effects distort the solitary wave on the primary flow in the same way, and begin to substantially modify the weakly nonlinear scaling at about the same level of axial velocity perturbation. These deviations from the weakly nonlinear scaling do not signal departures from solitary wave behavior, but rather transitions to a strongly nonlinear solitary wave regime. We note that for large perturbations, the L = 6 case falls on the same curve as the longer waves, implying that the period of this wave is not long enough to exhibit solitary wave behavior at small amplitude, but that it does develop strongly nonlinear solitary wave behavior at large amplitude.

(FIGURE 12 ABOUT HERE)

We conclude from these considerations that one wavelength of a periodic wavetrain rapidly approaches a solitary wave as the wave amplitude increases above a modest level. The resulting motion may be characterized either as weakly or as strongly nonlinear solitary waves, depending upon amplitude. Furthermore, the columnar flow to which these solitary waves tend, at distances from the station of maximum amplitude large compared to the half-length $L_{1/2}$, is not the specifying flow, but the principal conjugate flow. This point is illustrated in figure 13. Figure 13a shows the difference between the streamfunction of

principal conjugate flow and that of the first wavy branch as a function of r for wavelength L = 6 for three values (0.05, 0.25, and 1.0) of $(\Lambda - \mu_{(0)})/\mu_{(0)}$, corresponding the waves of increasing amplitude. At the largest $(\Lambda - \mu_{(0)})/\mu_{(0)}$ (hence the largest amplitude), the difference is barely detectable. Figure 13b shows the same tendency as L increases with the wave amplitude fixed.

(FIGURE 13 ABOUT HERE)

6. Solitary waves on the specifying flow

When the specifying flow is slightly supercritical, a weakly nonlinear solitary wave (29) is possible. A diagram summarizing the numerical continuation of this solitary wave solution branch to more strongly supercritical conditions (Λ decreasing from $\mu_{(0)}$; note that the scaled distance from the branch point, $|\Lambda - \mu_{(0)}|/\mu_{(0)}$, ranges from zero to a maximum of unity) is given in figure 14. The diagram superposes two measures of the wave disturbance of the specifying columnar flow, the maximum perturbation axial velocity (w'_{max}) at the plane of symmetry z = 0, and the perturbation axial velocity on the axis at this plane (w'(0,0)). The two measures agree for values of $|\Lambda - \mu_{00}|/\mu_{00}$ as large as 0.8. For larger values of this parameter, the point at which the perturbation axial velocity is a maximum lifts off of the rotation axis.

(FIGURE 14 ABOUT HERE)

The shift of the point of maximum axial velocity disturbance may also be seen in the axial velocity profiles at the symmetry plane. Profiles of the complete axial velocity component are drawn in figure 15 for four values of Λ. Three of the profiles include negative values of w, which implies the existence of a region of closed streamlines containing reversed axial velocities. When the maximum perturbation lifts off the axis, a high-speed upstream-directed jet forms in the interior of the recirculation region, and the dividing streamline develops a dimple at the axis and is no longer convex. We are unaware of observations of such a phenomenon, and believe it to be physically unrealizable.

(FIGURE 15 ABOUT HERE)

Projections of the streamlines onto the meridian plane are shown in figure 16. These plots show the emergence of the recirculation region. We have found that the flow field is represented with reasonable accuracy by the weakly nonlinear solution (29) for waves leading to axial velocity perturbations strong enough to cause flow reversal. This is

a significant finding, since we may then capture the essentials of our numerical computations of a strongly perturbed flow with the simple

(FIGURE 16 ABOUT HERE)

formula (29). To show the level of agreement, we have compared (for $\alpha = 14$) $w'(0,0)$ from our numerical computations with the approximation (29). This is found in figure 17, together with a comparison of the dependence of wave half-length with wave amplitude (measured by $w'(0,0)$ with the $-\frac{1}{2}$ power law dependence obeyed by the weakly nonlinear solitary wave. The weakly nonlinear solution (29) overpredicts the wave amplitude and length, but the differences are less than 10% for wave amplitudes large enough to cause stagnation and reversed axial flow.

(FIGURE 17 ABOUT HERE)

Contours of the perturbation streamfunctions, as predicted by numerical computation and by the weakly nonlinear approximation (29), are shown in figure 18. We judge the agreement to be qualitatively good for all three values of $|\Lambda - \mu_{00}|/\mu_{00}$ shown, quantitatively good for $|\Lambda - \mu_{00}|/\mu_{00} = 0.1$, and acceptable for some purposes for the higher values of $|\Lambda - \mu_{00}|/\mu_{00}$. It is worth noting that a stagnation point first appears in the flow for $|\Lambda - \mu_{00}|/\mu_{00} \approx 0.25$, so the three cases shown in figure 17 range from moderately to strongly nonlinear.

7. Discussion and Conclusions

We have shown here the connections between fully nonlinear standing periodic wavetrains and solitary waves and the underlying columnar flows. From a given primary, or "specifying", columnar flow, other columnar flows, solitary waves, and periodic wavetrains may be constructed. The solitary waves exist only when the primary flow is supercritical, a condition that arises when the swirl rate or axial vorticity in the primary flow is less than an easily determined critical value. Periodic wavetrains exist only when the primary flow is subcritical, which arises when the swirl rate exceeds the critical value. On the other hand, the periodic wavetrains rapidly attain the characteristics of solitary waves as the swirl, and with it the wave amplitude, increase for fixed wavelength; or as the wavelength increases at fixed, but finite, amplitude. These solitary waves do not propagate on the primary subcritical columnar flow. Instead, the flow far from the wave center is the principal conjugate columnar flow. The latter flow, in turn, connects to the primary flow at the critical swirl level, and as we show is supercritical when the primary flow is subcritical. Thus the requirement that flow upstream of solitary waves must be supercritical is maintained.

The simple, partly analytical, formula for weakly nonlinear solitary waves is shown to fit the numerical data for fully nonlinear solitary waves very well for a substantial range

of amplitudes. The errors associated with this fit are relatively small even for waves with amplitudes large enough to cause stagnation points and reversed axial flow to occur.

When stagnation points form, and with them recirculation regions of closed streamlines, we must face the special questions concerning the interpretation of the results. This is due to the well-known nonuniqueness of steady, axially symmetric, inviscid flows with closed streamlines. When closed streamsurfaces exist, the specification of the vorticity distribution by functional forms for $H'(\psi)$ and $F(\psi)$ determined by the upstream flow need not be continued into the region of closed streamlines. In fact, if the flow is to be steady *and* to be the limit of a viscous flow as the viscosity vanishes, the vorticity in the recirculation region must satisfy the constraint found by Prandtl (1904) and Batchelor (1956), which requires $F(\psi) \equiv 0$ and $H'(\psi) = \text{constant}$. One might think that a solution with closed streamlines, ignoring the Prandtl-Batchelor (or PB) condition, can be made consistent with it by recomputing the flow inside the dividing streamsurface, using the PB criterion to fix the interior vorticity distribution, but maintaining the exterior flow and the shape of the dividing streamsurface. This generally cannot be done, however, while balancing the interior and exterior pressures. Thus, if one insists on satisfying the PB condition, flows computed with an arbitrary specifying flow upstream must be discarded if recirculation appears unless a free streamline type of problem is solved in which the boundary shape between the external flow and the internal (PB flow) is part of the problem (see Leibovich, 1968 for an example of such a construction).

On the other hand, the PB criterion fails if the flow is not truly steady. (It also may fail in other circumstances, as described by Batchelor, 1956.) It is easy to imagine a nearly inviscid flow developing due to external forcing of various kinds, and then settling into a phase of very slow change. If closed streamlines are present, then viscous effects will act and cause the flow to vary with time. But this development is very slow, and so if one is interested in time intervals short compared to the viscous time (of order R^2/ν, where R is a length scale characterizing the recirculation region), then the PB condition does not constrain the vorticity distribution. The PB criterion also fails if the axial symmetry is lost (even if the nonaxially symmetric component of the flow is infinitesimally weak) since there is then fluid exchange across the nominal closed streamsurface. Our interest in vortex breakdown leads us to contemplate flows in which both of these conditions (external forcing driving flow axially-symmetric development of closed streamline regions on inertial time scales, followed by, or coincident with, symmetry breaking instability) are active. If an axially-symmetric recirculation zone existed and then was broken, the fluid exchange across the nominal boundary would, in our view, create an interior vorticity distribution that is not inconsistent with that in the external flow upstream. Thus the external form for $H'(\psi)$ would be reasonable in the interior (but the entire flow would of course be perturbed by the asymmetric motions), and a reasonable form for the circulation in the interior would be not $F(\psi)$ but $-F(\psi)$. This alteration is dynamically compatible with the flows computed here (as pointed out in *L*) and produces a flow with an interior swirl sense in agreement with that in the external flow, which is certainly required if there is exchange of fluid. Thus, it is our view that the flows calculated here having recirculation regions are sensible.

although possibly too simplistic, models of real vortex flows with stagnation points and a semblance of a recirculation region (albeit a broken one). We are in the process of exploring the breaking of the symmetry of these flows produced in this paper, and intend to report on that investigation in the future.

Acknowledgements

This work was supported by the U.S. Air Force Office of Scientific Research under grants AFOSR-87-0255 and AFOSR-89-0346, monitored by Dr. L. Sakell. Additional support was provided by the grant AFOSR-89-0226, monitored by Dr. J. McMichael, and by the U. S. Army Research Office at the Mathematical Sciences Institute of Cornell University.

Appendix: Numerical Implementation

A.1 Discretization

A finite-difference discretization is done on equation (16), written in the form:

$$D^2\Phi + \Omega(\Phi,r;\Lambda) = r\frac{\partial}{\partial r}\left(\frac{1}{r}\frac{\partial\Phi}{\partial r}\right) + \frac{\partial^2\Phi}{\partial z^2} - \Omega(\Phi,r;\Lambda) = 0 \qquad (A\,1)$$

The finite-difference approximation corresponding to this form of the radial derivatives has the property that the contribution of each cell boundary to the circulation around the cell is the same for the two cells adjacent at that boundary; the result is that any group of cells satisfy the Stokes theorem when individual cells do, similar to the flux consistency in "conservative" discretization of the Navier-Stokes or the energy equation.

We expect solutions that have sharp axial gradients, and non-uniform grid spacing may be necessary in the z-direction. This is done by defining a computational coordinate ζ, related to the physical coordinate z by $z=f(\zeta)$ ($f'(\zeta)\neq 0$); the z-derivative in (A1) becomes:

$$\frac{\partial^2\Phi}{\partial^2 z} = \frac{1}{f'(\zeta)}\frac{\partial}{\partial\zeta}\left(\frac{1}{f'(\zeta)}\frac{\partial\Phi}{\partial\zeta}\right)$$

Equation (A1) is discretized by central differences on a rectangular grid having uniform spacing in (r,ζ), corresponding to variable spacing in z. The finite-dimensional version of equation (A1) is—

$$\underline{D}\,\underline{\Phi} + \underline{\Omega}(\underline{\Phi},\Lambda) = 0 \qquad (A\,2)$$

where:

$$(\underline{\Phi})_{ij} \equiv \Phi(r_i, \zeta_j)$$

$$(\underline{\Omega})_{ij} \equiv \Lambda\,(\underline{P})_{ij} + (\underline{Q})_{ij} \equiv \Lambda\,P((\underline{\Phi})_{ij}) - r_i^2\,Q((\underline{\Phi})_{ij})$$

$$\underline{D} \equiv \underline{D}^r + \underline{D}^z$$

$$(\underline{D}^r)_{rsij} = \begin{cases} \Delta r^{-2}\left(1-\frac{\Delta r}{2r_p}\right)^{-1} & j=q \text{ and } i=p-1 \\ -2\Delta r^{-2}\left(1-\left(\frac{\Delta r}{2r_p}\right)^2\right)^{-1} & j=q \text{ and } i=p \\ \Delta r^{-2}\left(1+\frac{\Delta r}{2r_p}\right)^{-1} & j=q \text{ and } i=p+1 \\ 0 & \text{otherwise} \end{cases}$$

$$(\underline{D}^{\zeta})_{pqij} = \begin{cases} \Delta\zeta^{-2}\,[f'(\zeta_q)\,f'(\zeta_q-\Delta\zeta/2)]^{-1} & i=p \quad j=q-1 \\ -\Delta\zeta^{-2}\,f'(\zeta_q)^{-1}\,[f'(\zeta_q+\Delta\zeta/2)^{-1}+f'(\zeta_q-\Delta\zeta/2)^{-1}] & i=p \quad j=q \\ \Delta\zeta^{-2}\,[f'(\zeta_q)\,f'(\zeta_q+\Delta\zeta/2)]^{-1} & i=p \quad j=q+1 \\ 0 & \text{otherwise} \end{cases}$$

$\underline{D}^{r}$, $\underline{D}^{\zeta}$ are "directional operators", containing entries relevant to the derivatives in r, ζ directions. Each contains three nonzero diagonals in a block structure as shown in figure A1. The separation of $\underline{D}$ into its directional components and the structure of these components will be used in section A.2 below to form efficient and consistent concepts of separation of variables and inner product for the discrete problem A2.

(FIGURE A1 ABOUT HERE)

The contribution of boundary points with Dirichlet type boundary condition is placed in $\underline{\Omega}$ when non-zero; for Neumann type boundary condition, an external node is defined outside the boundary, its value given by the first derivative at the boundary; for $\frac{d\Phi}{dn}=0$, we set $\Phi_{\beta+1}=\Phi_{\beta-1}$ in the equation for the boundary node Φ_β. The singularity of (A1) at r=0 is not explicitly present in the numerical problem, since Φ=0 at r=0, and the discretization of (A1) takes place only in the interior of the domain—*a finite distance from r=0 (more on this* singularity in section A.4).

A.2 Algebraic Treatment of the Bifurcation and Continuation

In the neighborhood of any bifurcation point Λ=μ, we expand the solution to (A2) in a small parameter ε, as in (18):

$$\underline{\Phi} = \varepsilon\,\underline{\varphi}_0 + \varepsilon^2\,\underline{\varphi}_1 + \ldots \qquad (A3)$$

$$\Lambda = \mu + \varepsilon\,\kappa_0 + \varepsilon^2\,\kappa_1 + \ldots$$

Substituting into (A2) and collecting terms of like power in ε, we obtain the sequence of equations, analogous to (20), the first three of which are:

$$\underline{L}\,\underline{\varphi}_0 \equiv [\,\underline{D} + \mu\,\underline{P}^{(1)} + \underline{Q}^{(1)}\,]\,\underline{\varphi}_0 = [\,\underline{D} + \underline{S}^{(1)}\,]\,\underline{\varphi}_0 = 0 \qquad (A4a)$$

$$\underline{L}\,\underline{\varphi}_1 = -\kappa_0\,\underline{P}^{(1)}\underline{\varphi}_0 - \underline{S}^{(2)}\,\underline{\varphi}_0\,\underline{\varphi}_0 \qquad (A4b)$$

$$\underline{L}\,\underline{\varphi}_2 = -\kappa_1\underline{P}^{(1)}\underline{\varphi}_0 - \kappa_0\underline{P}^{(1)}\underline{\varphi}_1 - 2\underline{S}^{(2)}\underline{\varphi}_0\underline{\varphi}_1 - \underline{S}^{(3)}\underline{\varphi}_0\underline{\varphi}_0\underline{\varphi}_0 - \kappa_0\underline{P}^{(2)}\underline{\varphi}_0\underline{\varphi}_0 \qquad (A4c)$$

where the derivatives of $\underline{\Omega}$ are defined following (19):

$$(\underline{P}^{(1)})_{pqij} = \frac{\partial(\underline{P})_{pq}}{\partial(\underline{\Phi})_{ij}}(\underline{\Phi}=0) \quad , \quad (\underline{P}^{(2)})_{pqijkl} = \frac{\partial^2(\underline{P})_{pq}}{\partial(\underline{\Phi})_{ij}\,\partial(\underline{\Phi})_{kl}}$$

$$(\underline{\Phi}=0) \quad , \quad \ldots$$

$$(\underline{Q}^{(1)})_{pqij} = \frac{\partial(\underline{Q})_{pq}}{\partial(\underline{\Phi})_{ij}}(\underline{\Phi}=0) \quad , \quad (\underline{Q}^{(2)})_{pqijkl} = \frac{\partial^2(\underline{Q})_{pq}}{\partial(\underline{\Phi})_{ij}\,\partial(\underline{\Phi})_{kl}}$$

$$(\underline{\Phi}=0) \quad , \quad \ldots$$

$$\underline{S}^{(k)} \equiv \mu\,\underline{P}^{(k)} + \underline{Q}^{(k)}$$

The eigenvalue problem (A4a) can be solved by separation of variables: let $\underline{\varphi}_0$ have the form, equivalent to (21)

$$(\underline{\varphi}_0)_{ij} = (\underline{\varphi}_0^r)_i\,(\underline{\varphi}_0^z)_j$$

where $\underline{\varphi}_0^r$ and $\underline{\varphi}_0^z$ may be called "directional" components of $\underline{\varphi}_0$. Substituting into (A4a) and using the repeated block structure of $\underline{D}$ we obtain:

$$\{[(\underline{D}^r)_{p1i1} + \mu(\underline{P}^{(1)})_{p1i1} + (\underline{Q}^{(1)})_{p1i1}](\underline{\varphi}_0^r)_i\}\,(\underline{\varphi}_0^z)_q + (\underline{\varphi}_0^r)_p\,\{(\underline{D}^z)_{1q1j}(\underline{\varphi}_0^z)_j\} = 0$$

which is an equality of two rank-1 matrices: there exists therefore a scalar β such that:

$$-\beta\,(\underline{\varphi}_0^z)_q + (\underline{D}^z)_{1q1j}(\underline{\varphi}_0^z)_j = 0 \qquad \text{(A 5a)}$$

and:

$$\underline{P}^{(1)-1}_{ip1}\{(\underline{D}^r)_{p1i1} + \beta\,\underline{I}_{p1i1} + (\underline{Q}^{(1)})_{p1i1}\}(\underline{\varphi}_0^r)_i + \mu\,(\underline{\varphi}_0^r)_p = 0 \qquad \text{(A 5b)}$$

Note that $\underline{P}^{(1)}$ is invertible since it is a diagonal matrix having $p(r_i)$ entries on its diagonal, which are positive.

The eigenvalues β_n, μ_{nm} and their eigenvectors are found from (A5) by the tridiagonal set of subroutines from Eispack.

Define an inner product as follows:

$$\langle \underline{x}\,,\,\underline{y} \rangle = \underline{x}^T\,\underline{S}\,\underline{y} \qquad \text{(A 6)}$$

where:

$$(\underline{S})_{pqij} = (\underline{S}^r)_{pi}\,(\underline{S}^z)_{qj}$$

and $\underline{S}^r$, $\underline{S}^z$ are diagonal: $\underline{S}^r = \mathrm{diag}\left[\frac{p(r_i)}{r_i}\right]$, $\underline{S}^z = \mathrm{diag}\left[f'(\zeta_i)\right]$ (the first and last elements may be different due to the boundary conditions); both are positive definite. Under this inner product, $(\underline{P}^{(1)})^{-1}\underline{L}$ is self-adjoint and the eigenvectors of (A4a) are orthogonal.

Multiply (A4b) by $(\underline{P}^{(1)})^{-1}$ to obtain the self-adjoint form of the operator, and we can impose a solvability condition:

$$< (\underline{P}^{(1)})^{-1} [\underline{S}^{(2)}\, \underline{\varphi}_0\, \underline{\varphi}_0 + \kappa_0\, \underline{P}^{(1)}\, \underline{\varphi}_0] , \underline{\varphi}_0 > = 0 \qquad (A\,7)$$

This is used to find κ_0, as in (23). To solve (A4b) for $\underline{\varphi}_1$, we use an eigenvector expansion method. Similarly, κ_1 and $\underline{\varphi}_2$ can be found from (A4c), and so on to any desired order. We used two or three terms of (A3), depending on the type of bifurcation encountered.

Let $\dot{\underline{\Phi}} \equiv \frac{\partial \underline{\Phi}}{\partial \Lambda}$, and take the derivative of (A2) with respect to Λ:

$$\underline{L}\, \dot{\underline{\Phi}} = - \underline{P}(\underline{\Phi}) \qquad (A8)$$

This is a system of ODE's for $\underline{\Phi}(\Lambda)$, equivalent to (29b); given initial conditions $\underline{\Phi}(\Lambda_0)$ from (A3) or the weakly-nonlinear estimate (30), this linear system can be solved for $\dot{\underline{\Phi}}$. We use Sparspak (George et al. 1980) to solve (A8) and a Runge-Kutta integrator (Press et al. 1986) to integrate over Λ.

Given $\underline{\Phi}_0$ and Λ, an approximate solution of (A2), we may define a Newton's Method iteration [Dennis & Schnabel, 1983]:

$$\underline{\Phi}_{k+1} = \underline{\Phi}_k - [\underline{D}+\Lambda \underline{P}_k^{(1)}+\underline{Q}_k^{(1)}]^{-1} [\underline{D}\, \underline{\Phi}_k+\underline{\Omega}(\underline{\Phi}_k ,\Lambda)] \qquad (A\,9)$$

where:

$$(\underline{P}_k^{(1)})_{pqij} = \frac{\partial (\underline{P})_{pq}}{\partial (\underline{\Phi})_{ij}} (\underline{\Phi}=\underline{\Phi}_k)$$

$$(\underline{Q}_k^{(1)})_{pqij} = \frac{\partial (\underline{Q})_{pq}}{\partial (\underline{\Phi})_{ij}} (\underline{\Phi}=\underline{\Phi}_k)$$

Under some mild assumptions, in particular that $\underline{\Phi}_0$ be close enough to the exact solution and that the Jacobian be nonsingular and Lipschitz continuous, this iteration will converge to the exact solution at quadratic rate [Dennis & Schnabel, theorem 5.2.1]. If we make the initial estimate (A3) and the integration (A8) accurate enough and stay away from bifurcation points (where the Jacobian is singular), then convergence of this step is practically guaranteed.

We use Sparspak to solve each step of (A9), and a line search algorithm to improve global convergence properties. The structure of the Jacobian in (A9) is the same as that of $\underline{L}$ in (A8), so the most time-consuming part of the Sparspak algorithm—the structure decomposition—needs to be done only once.

A.3 Numerical Errors and Convergence

Two types of numerical errors need to be considered: the discretization error (the difference between the exact analytic solution and the exact solution of the discretized system), and the convergence error (the difference between the numbers actually obtained and the exact solution of the discretized problem). Convergence errors are important in the corrector step only since those occurring in the predictor steps—initial estimate and integration—are irrelevant when the corrector step converges.

The initial estimate need not be very accurate, as explained above. However, if it is too inaccurate, then the corrector procedure may converge to a different branch or not converge to a solution at all. The initial estimate will improved as $\varepsilon \to 0$ in (A3), but the integration and corrector steps will lose accuracy as the Jacobian becomes singular near the bifurcation point. We found that with $\varepsilon=0.01$, taking up to 3 terms of the series (A3) leads to convergence of (A9) and reasonable accuracy for the subsequent integration.

The convergence errors are determined by the stopping criterion of the corrector step (A9):

$$\| \underline{\mathbf{D}}\,\underline{\Phi} + \underline{\Omega}(\underline{\Phi},\Lambda) \|_{\zeta}^{2} \le \delta^2$$

The change in $\|\underline{\Phi}\|$ in the last Newton step is usually considered to be of the same order as the convergence error. For $\delta=10^{-8}$, the typical value was: $\| \Delta\underline{\Phi} \| \approx 10^{-5}$. As shown below, this is much smaller than the estimate for the discretization error, and we may therefore treat the computed solutions as "exact" solutions of the discretized problem.

Equation (A2) was derived using central differences, and is second-order correct in Δr, $\Delta\zeta$. The grid transformations $z \to \zeta$ used have a finite derivative everywhere, and therefore do not effect the order of the truncation error (Kalnay de Rivas, 1972); therefore it is considered second-order also in Δz. Higher-order accuracy, as well as an estimate for the discretization error, may be obtained by Richardson's Extrapolation. Computation was repeated for sample cases with grids having resolutions of (N_r,N_z), where N_r & $N_z \in$ (10,20,40): 9 different grids, followed by a 2-dimensional extrapolation to $\frac{1}{N} \to 0$. Typical values of the relative difference of the second-order solution from the extrapolated results are presented in figure A2: these differences serve as an estimate for the discretization error.

(FIGURE A2 ABOUT HERE)

To further validate the above estimate of the discretization error, we applied the numerical algorithm to a problem having a known solution. The nonlinear function Ω in equation (16) is chosen to be:

$$\Omega(\Phi,r;\Lambda) = \Lambda\Phi + \frac{\Phi^2}{r\,J_1(a\,r)}$$

where J_1 is a Bessel function of order 1 and a is its first zero (a =3.8317.....). Equation (16) with this Ω has an analytic solution which is qualitatively similar to the computed (and weakly nonlinear) solitary waves:

$$\Phi(r,z) = \frac{3}{2}(a^2-\Lambda)\, r\, J_1(a\, r)\, \mathrm{sech}^2\left(\frac{1}{2}\, z\, \sqrt{a^2-\Lambda}\right)$$

This solution bifurcates from the trivial Φ=0 branch at $\Lambda=a^2$ and increases in magnitude as $\Lambda\rightarrow 0$. (This problem does not necessarily correspond to a physical primary flow.) The discretization errors for Φ, μ_{00}, μ_{01} and the first two axial wavenumbers are presented in figure A3.

(FIGURE A3 ABOUT HERE)

The error in the perturbation streamfunction with the 20x20 grid is close to 2% for the test function and less than 1% for the Richardson-extrapolated case. For velocities (computed from the streamfunction by central differences), the discretization error is larger, but still not exceeding a few percent on a 20x20 grid. The results in figure A2(b) are for the axial velocity $w=\partial\psi/r\partial r$, which is strongly dependent on r-resolution. The errors in the values of the axial wavenumbers $\sqrt{\beta_n}$ and the bifurcation points μ_{nm} are similarly of order 1% for the same level of resolution. The 20x20 grid was therefore the standard in most of our computations.

A.4 The Singularity at r=0

Equation (16) has a singularity on the axis r=0, and construction of a numerical scheme as well as interpretation of the results should take that singularity into account. The discretization (A2) makes explicit use of the boundary condition (16c) at r=0, and applies (A1) only to interior grid points; the singularity is thus avoided. However, if the grid is refined until $\frac{1}{r}$ becomes very large at the first grid point off the axis, then the matrices involved will become unbalanced and numerical accuracy will deteriorate. In our case such fine grids are not necessary since Richardson's extrapolation seems to show convergence before very large numbers occur.

The singularity is encountered again when we compute the axial velocity at the axis, which is used as a measure of the perturbation size. The definition: $w=r^{-1}\partial\psi/\partial r$ cannot be applied directly at r=0; two numerical schemes are used, and the values obtained for w(0,0) agree to within a few percent.

The first method is a quadratic extrapolation of w values from interior grid points, coupled with the condition: $\partial w/\partial r$=0 at r=0. The quadratic function satisfying this condition and passing through the first two interior grid points is:

$$\tilde{w}(r) = \frac{1}{3}\, w(\Delta r)\left[4-\left(\frac{r}{\Delta r}\right)^2\right] + \frac{1}{3}\, w(2\Delta r)\left[\left(\frac{r}{\Delta r}\right)^2-1\right]$$

leading to:

$$\tilde{w}(0) = \frac{4w(\Delta r) - w(2\Delta r)}{3}$$

The second method applies Stokes' theorem to a rectangular loop of dimensions (δr, δz) touching the axis r=0 and centered about the line of symmetry z=0. To reduce the error associated with numerical integration over a finite rectangle, we let $\delta z \to 0$ and obtain a balance involving r-integration only. The vorticity integral can be expanded in powers of δz, η being the azimuthal component of the vorticity:

$$\int_S \omega \bullet ds = \int_0^{\delta r} \int_{-\delta z/2}^{\delta z/2} \left[\eta(r,0) + z\frac{\partial \eta}{\partial z}(r,0) + \ldots \right] dz\, dr$$

$$= \delta z \int_0^{\delta r} \eta(r,0)\, dr + O(\delta z^2)$$

A similar expansion is done for the circulation integrals:

$$\oint \mathbf{u} \bullet d\mathbf{l} = \int_{-\delta z/2}^{\delta z/2} [w(0,z) - w(\delta r,z)]\, dz$$

$$+ \int_0^{\delta r} [u(r,\delta z/2) - u(r,-\delta z/2)]\, dr$$

$$= \delta z \left[w(0,0) - w(\delta r,0) - \int_0^{\delta r} \frac{1}{r}\frac{\partial^2 \psi}{\partial z^2}(r,0)\, dr \right] + O(\delta z^2)$$

Comparing the leading terms in δz, we obtain:

$$w(0,0) = w(\delta r,0) + \int_0^{\delta r} \left[\eta(r,0) + \frac{1}{r}\frac{\partial^2 \psi}{\partial z^2}(r,0) \right] dr$$

The integral was computed using the Simpson $\frac{1}{3}$-rule, and the two expressions for w(0,0) were compared for $\delta r = \Delta r$ and $2\Delta r$. The differences were of order 1% in most cases, and increased up to 5% only as $\Lambda \to \mu$ (where the perturbation is small and roundoff error becomes significant) and as $\Lambda \to 0$ (where large radial gradients require increased resolution). We therefore used the simpler quadratic extrapolation form throughout. This comparison also serves as an additional check on the convergence of the numerical results near the singular line r=0.

References

Batchelor, G.K. 1956 On steady laminar flow with closed streamlines at large Reynolds number. *J. Fluid Mech.*, **1**, 177-190.

Batchelor, G.K. 1967 *Introduction to Fluid Mechanics*, Cambridge University Press

Benjamin, T. B. 1962 Theory of the vortex breakdown phenomenon. *J. Fluid Mech.*, **14**, 593-629.

Benjamin, T. B. 1967 Some developments in the theory of vortex breakdown. *J. Fluid Mech.*, **28**, 65-84.

Bragg, S.L. & Hawthorne, W.R. 1950 Some exact solutions of the flow through annular cascade actuator discs. *J. Aero. Sci.*, **17**, 243-249.

Buckmaster, J.S. & Ludford, G.S.S. 1982 *Theory of Laminar Flames*, Cambridge University Press.

Courant, R. & Hilbert, D. 1953 *Methods of Mathematical Physics*, Vol. 1, Interscience, New York

Dennis, J.E. & Schnabel, R.B. 1983 *Numerical Methods for Unconstrained Optimization and Nonlinear Equations* , Prentice–Hall.

Dongarra, J.J. 1979 *Linpack User's Guide* , Society for Industrial and Applied Mathematics.

Faler, J.H. & Leibovich, S. 1977 Disrupted states of vortex flow and vortex breakdown. *Physics of Fluids*, **20**, 1385-1400.

Faler, J.H. & Leibovich, S. 1978 An experimental map of the internal structure of a vortex breakdown. *J. Fluid Mech.*, **86**, 313-335.

Frankel, L.E. 1956 On the flow of rotating fluid past bodies in a pipe. Proc. Roy. Soc.A **233**, 506-526.

Garg, A.K.& Leibovich, S. 1979 Spectral characteristics of vortex breakdown flowfields *Physics of Fluids*, **22**, 2053-2064.

George, A. et al. 1980 *User Guide for SPARSPAK* , University of Waterloo.

Hafez, M. & Salas, M. 1985 Vortex breakdown simulation based on a nonlinear inviscid model.Chapter in *Studies of Vortex Dominated Flows*, ed. by M.Y. Hussaini and M.D. Salas, 76-82.

Hafez, M., Ahmad, J., Kuruvila, G., & Salas, M. D. 1987 Vortex breakdown simulation, AIAA 87-1343, Honolulu, Hawaii.

Howard, L. & Gupta, A.S. 1962 On the hydrodynamic and hydromagnetic stability of swirling flows, *J. Fluid Mech.* **14**, 463-476.

Kalnay de Rivas, E. 1972 On the use of nonuniform grids in finite-difference equations. *J. of Computational Physics* **10**, 202-210

Keller, H.B. 1977 Numerical solution of bifurcation and nonlinear eigenvalue problems. In *Applications of Bifurcation Theory* , P.H. Rabinowitz (ed.), Academic Press, New York, 359-384

Kubicek, M. & Marek, M. 1983 *Computational Methods in Bifurcation Theory and Dissipative Structures*, Springer-Verlag, New York.

Leibovich, S. 1968 Axially-symmetric eddies embedded in a rotational stream, *J. Fluid Mech.*, **32**, 529-548.

Leibovich, S. 1970 Weakly nonlinear waves in rotating fluids, *J. Fluid Mech.*, **42**, 803-822.

Leibovich, S. 1978 The structure of vortex breakdown, *Ann. Rev. Fluid Mech.*, **10**, 221-246.

Leibovich, S. 1979 Waves in parallel or swirling stratified shear flows, *J. Fluid Mech.*, **93**, 401-412.

Leibovich, S. 1983 Vortex stability and breakdown. In: *Aerodynamics of Vortical Type Flows in Three Dimensions*, A. D. Young, ed., *AGARD Conference Proceedings* **No. 342** (NATO), 23.1-23.22.

Leibovich, S. 1984 Vortex stability and breakdown: Survey and extension, *AIAA J.* **22**, 1192-1206.

Leibovich, S. 1985 Waves and bifurcations in vortex filaments, Chapter in *Studies of Vortex Dominated Flows*, ed. by M.Y. Hussaini and M.D. Salas, 3-15.

Leibovich, S., Brown, S.N., & Patel, Y. 1986 Bending waves on inviscid columnar vortices *J. Fluid Mech.*, **173**, 595-624.

Leibovich, S. 1987 Fully nonlinear structures, wavetrains, and solitary waves in vortex filaments. In *Nonlinear Wave Interactions in Fluids*, ed. by R.W. Miksad, T.R. Akylas, and T. Herbert, 67-70.

Long, R.R. 1953 Steady motion around asymmetrical obstacle moving along the axis of a rotating liquid. *J. Meteor.*, **10**, 197-203.

Maxworthy, T., Mory, & Hopfinger, E. 1983 Waves on vortex cores and their relation to vortex breakdown. In: *Aerodynamics of Vortical Type Flows in Three Dimensions*, A. D. Young, ed., *AGARD Conference Proceedings* **No. 342** (NATO), Paper 29.

Prandtl, L. 1904 Über Flüssigkeitsbewegung bei sehr kleiner Reibung, *3rd Inter.Congress of Mathematicians* (Heidelberg), B.G. Teubner, Leipzig, pp.484-491.

Press, W.H. et al. 1986 *Numerical Recipes* , Cambridge University Press.

Randall, J. D. & Leibovich, S. 1973 The critical state: A trapped wave model of vortex breakdown, *J.Fluid Mech.* **53**, 481-493.

Rayleigh, Lord 1916 On the stability, or instability, of certain fluid motions, *Proc. Roy. Soc Lon.* **A93**, 148-154.

Sarpkaya, T. 1971 On stationary and travelling vortex breakdowns, *J. Fluid Mech.* **45**, 545-559.

Smith, B.T. et al. 1976 *Matrix Eigensystem Routines— EISPACK Guide, 2nd ed.* , vol. 6 of *Lecture Notes in Computer Science* , Springer-Verlag.

Smith, G.D. 1985 *Numerical Solution of Partial Differential Equations: Finite Difference Methods* , Clarendon Press.

Squire, H.B.1956 Rotating Fluids, Chapter in *Surveys in Mechanics*, ed. G.K. Batchelor and R. M. Davies, Cambridge University Press.

Synge, J.L. 1933 The stability of heterogeneous liquids, *Trans. Roy. Soc. Canada* **27**, 1-18.

Szeri, A. J. 1988, *Nonlinear Stability of Axisymmetirc Swirling Flow*, PhD Dissertation, Cornell University, Ithaca, NY.

Yih, C.S. 1965 *Dynamics of Nonhomogeneous Fluids*, Academic Press.

Figure Captions

Figure 1. Bifurcation diagram for the first two columnar branches. The extreme perturbation axial velocity occurs away from the axis on part of the second branch.

Figure 2. Velocities on the second columnar branch, for different values of the swirl parameter Λ. (a) axial velocity (b) azimuthal velocity.

Figure 3. Velocities on the supercritical side of the principal columnar branch. (a) axial velocity (b) azimuthal velocity.

Figure 4. Velocities on the subcritical side of the principal columnar branch. (a) axial velocity (b) azimuthal velocity.

Figure 5. Exchange of criticality between the primary flow (—o—) and the principal conjugate branch (—●—), using Benjamin's Froude number criterion.

Figure 6. Comparison of computed (o) and asymptotic (—) solutions in the limit $\Lambda \to 0$ on the principal branch. (a) location of the boundary layer (b) maximum of the streamfunction ψ_* (c) layer thickness δ.

Figure 7. Comparison of computed and asymptotic velocity profiles for the principal branch, at $\Lambda = 0.001\mu_{00}$.

Figure 8. Bifurcation diagram for the periodic branches of μ_{01} and μ_{02} ; $\alpha=2$ for better separation of the bifurcation points. —— principal columnar branch : —o— L=10 wave centered at z=L/2; —●— L=10 wave centered at z=0; —□— L=5 wave centered at z=L/2; —■— L=5 wave centered at z=0.

Figure 9. Approach of the periodic solutions to localized waves. (a) fixed length L=6: wave trough becomes localized as the wave amplitude increases. (b) fixed amplitude $\Lambda/\mu=1.10$: the half-height-length of the wave approaches a constant value independent of the computational domain length.

Figure 10. Meridional streamlines of periodic solutions: L=3, $\alpha=14$, contour intervals of 0.1 . (a) $(\Lambda-\mu)/\mu=1.5$, just before the appearance of stagnation points. (b) $(\Lambda-\mu)/\mu=1.6$, a recirculation bubble appears. (c) $(\Lambda-\mu)/\mu=2.5$, the recirculation region grows with the perturbation amplitude. (d) detail of the bubble in (c).

Figure 11. Velocities on the periodic branch of μ_{01} at the wave center z=0. (a) axial velocity (b) azimuthal velocity (c) difference in axial velocity between the wave center and tail.

Figure 12. Solitary wave behaviour of the periodic solutions: the dependence of effective wave length (half-height length) on the wave amplitude, compared to the -0.5 slope for an exact solitary wave. o L=6; • L=20; + L=100. (a) wave amplitude measured by extreme axial velocity (b) wave amplitude measured by the distance from the bifurcation point.

Figure 13. Convergence of the wave crests of the periodic solution to the columnar solution of the same amplitude. (a) fixed length L=6, the difference vanishes as the wave amplitude increases. (b) fixed amplitude $(\Lambda-\mu_{01})/\mu_{01}=0.05$, as the computational domain length increases.

Figure 14. Bifurcation diagram, solitary wave branch. The extreme perturbation axial velocity is off the axis when $\Lambda<0.16\mu_{00}$.

Figure 15. Axial velocity at wave center z=0 on the solitary wave branch

Figure 16. Meridional streamlines of solitary wave solutions, L=5, contour intervals 0.05. (a) $\Lambda/\mu_{00}=0.80$ (b) $\Lambda/\mu_{00}=0.70$, a small recirculation bubble appears (c) $\Lambda/\mu_{00}=0.001$, a large recirculation bubble. (d) detail of the bubble in (b), (e) detail of the bubble in (c).

Figure 17. Comparison of solitary wave amplitude of the computed (o) and weakly-nonlinear (—) solutions. (a) bifurcation diagram (b) detail showing the bifurcation and the amplitudes of flow reversal. (c) half-height-length vs. amplitude of the computed wave, compared to the -0.5 slope of the exact solitary wave.

Figure 18. Comparison of perturbation streamlines of the computed (—) vs. the weakly-nonlinear (·····) solitary waves. (a) $\Lambda/\mu_{00}=0.90$, contour intervals 0.004 (b) $\Lambda/\mu_{00}=0.50$, contour intervals 0.012 (c) $\Lambda/\mu_{00}=0.20$, contour intervals 0.02 .

Figure A1. Structure of the matrices (a) D^{r}_{pqij} (b) D^{z}_{pqij}.

Figure A2. Variation with mesh size of errors relative to Richardson-extrapolated values at $\Lambda/\mu_{00}=0.80$: • actual computation with this mesh; o extrapolated. (a) error in $\Phi(0.3,0)$ (b) error in $w(0,0)$ (c) error in μ_{00}.

Figure A3. Variation with mesh size of errors relative to the exact solution of the test problem: ● actual computation with this mesh; o extrapolated. (a) maximum error in $\Phi(r,z)$ at $\Lambda/a^2=0.80$. (b) error in axial wavenumbers. (c) error in μ_{03}. (d) error in μ_{01}.

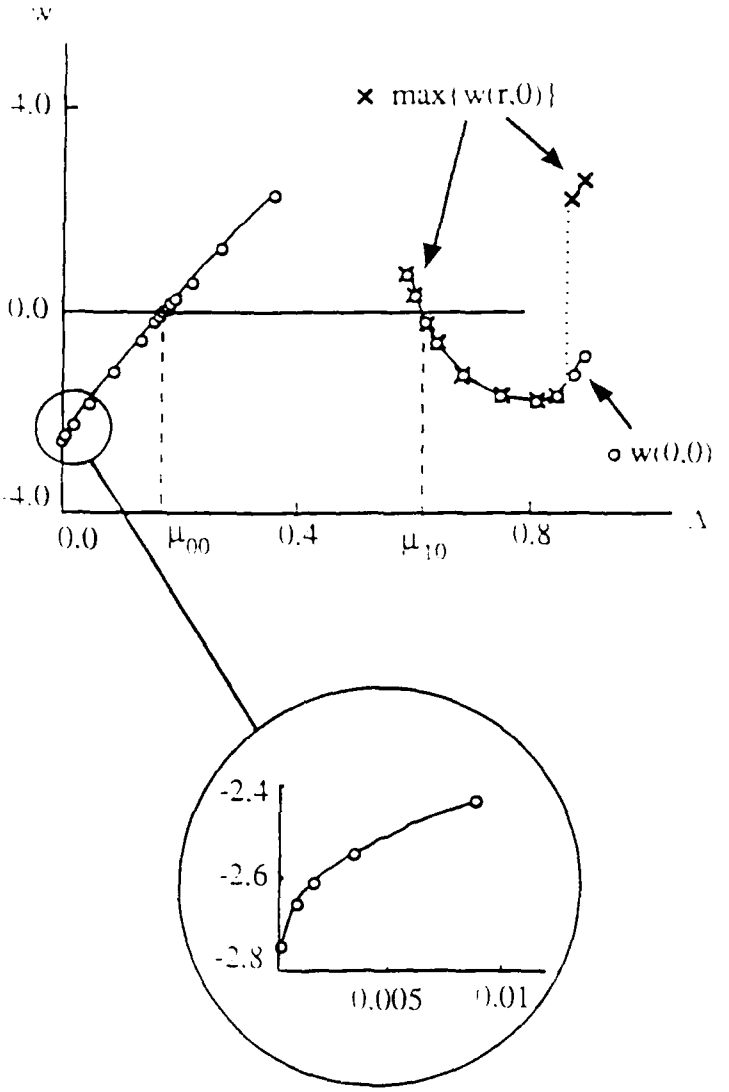

Figure 1

(a)

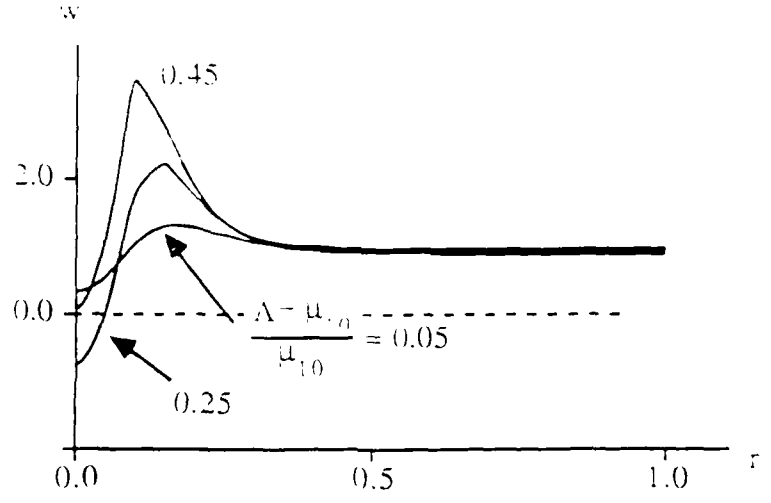
v
0.45
2.0
0.0
$\frac{\Lambda - \mu_{10}}{\mu_{10}} = 0.05$
0.25
0.0
0.5
1.0
t

(b)

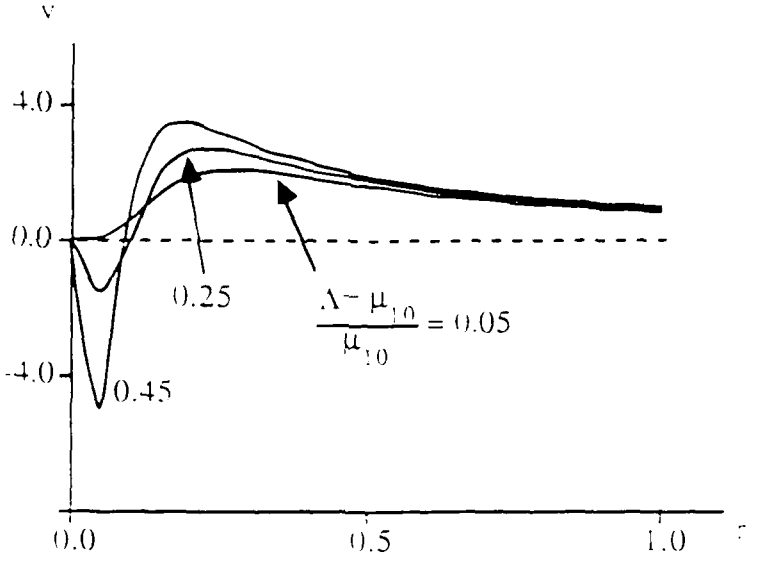
v
4.0
0.0
-4.0
0.25
$\frac{\Lambda - \mu_{10}}{\mu_{10}} = 0.05$
0.45
0.0
0.5
1.0
t

Figure 2

(a)

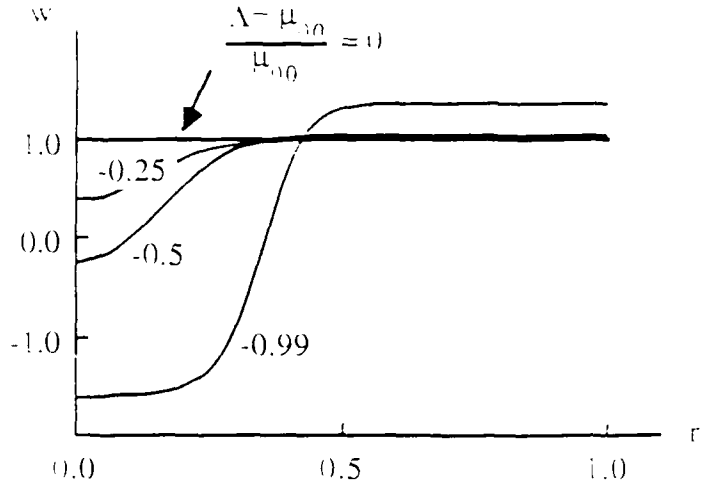
W
$\frac{\Lambda - \mu_{00}}{\mu_{00}} = 0$
1.0
0.0
-1.0
-0.25
-0.5
-0.99
r
0.0
0.5
1.0

(b)

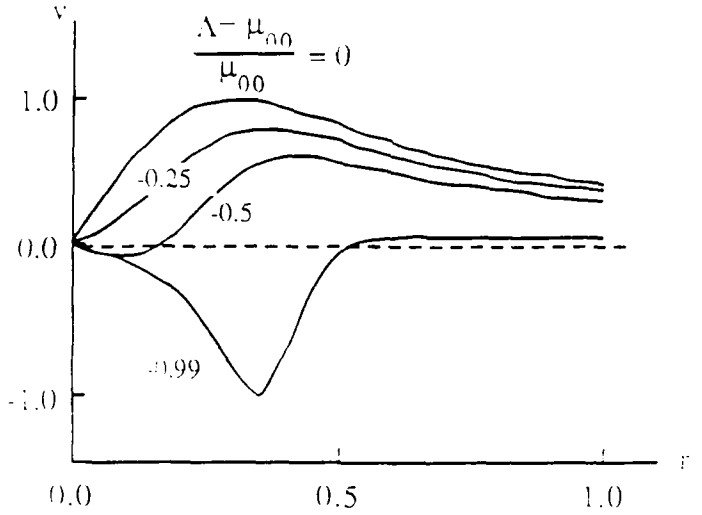
V
$\frac{\Lambda - \mu_{00}}{\mu_{00}} = 0$
1.0
0.0
-1.0
-0.25
-0.5
-0.99
r
0.0
0.5
1.0

Figure 3

(a)

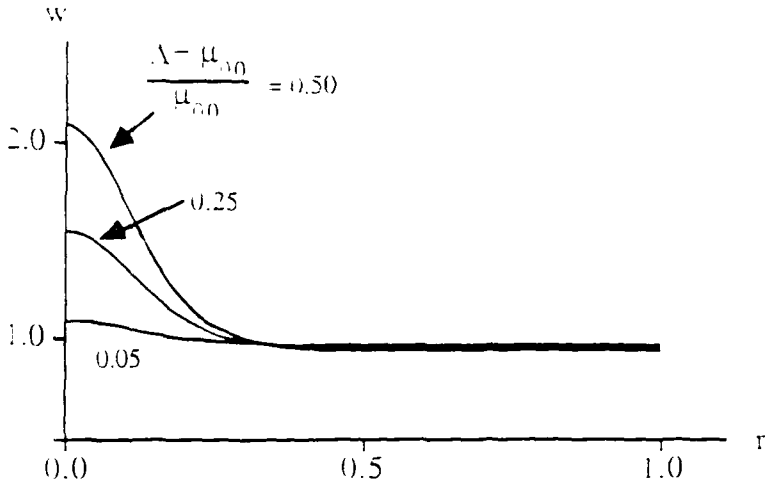
w
$\frac{\Lambda - \mu_{00}}{\mu_{00}} = 0.50$
0.25
0.05
2.0
1.0
0.0
0.5
1.0
r

(b)

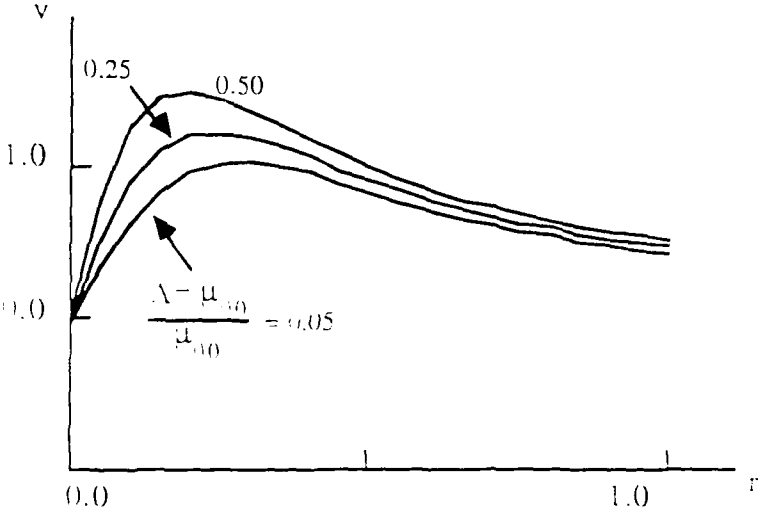
v
0.25
0.50
1.0
$\frac{\Lambda - \mu_{00}}{\mu_{00}} = 0.05$
0.0
1.0
r

Figure 4

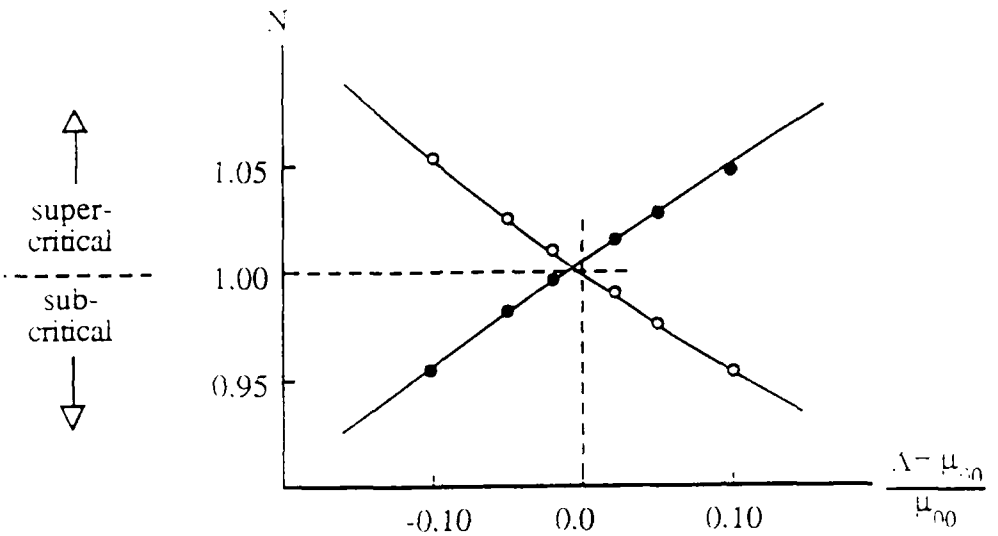

Figure 5

(a)

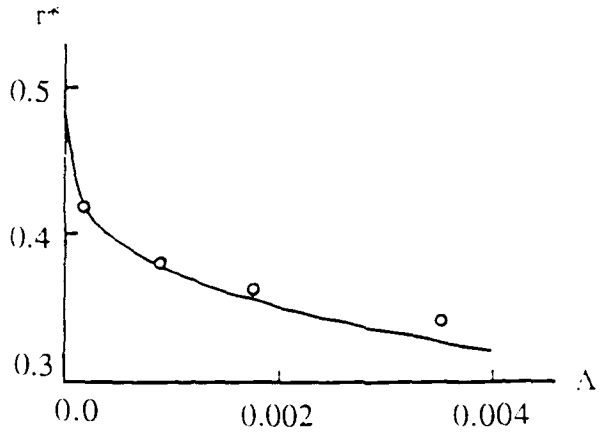
r*
0.5
0.4
0.3
A
0.0
0.002
0.004

(b)

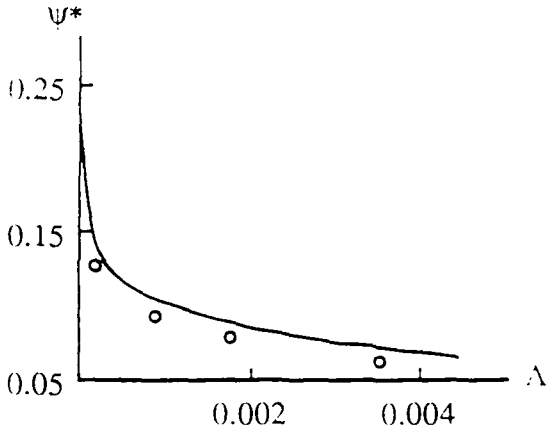
ψ*
0.25
0.15
0.05
A
0.002
0.004

(c)

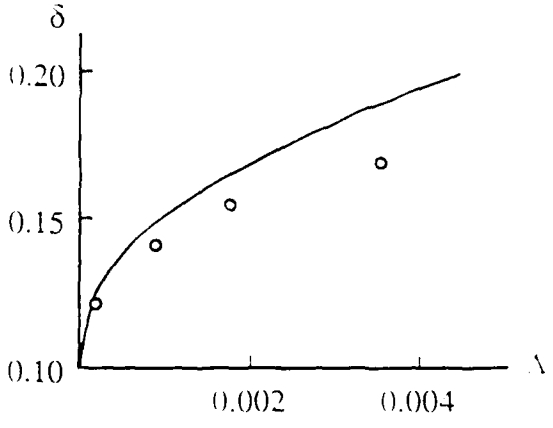
δ
0.20
0.15
0.10
A
0.002
0.004

Figure 6

(a)

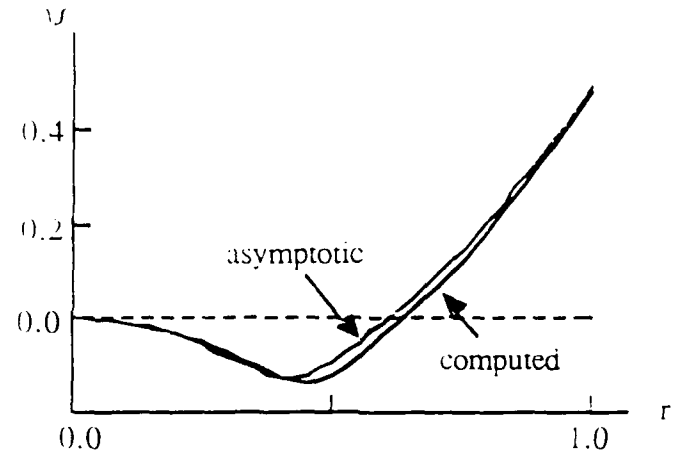
v
0.4
0.2
0.0
asymptotic
computed
r
0.0
1.0

(b)

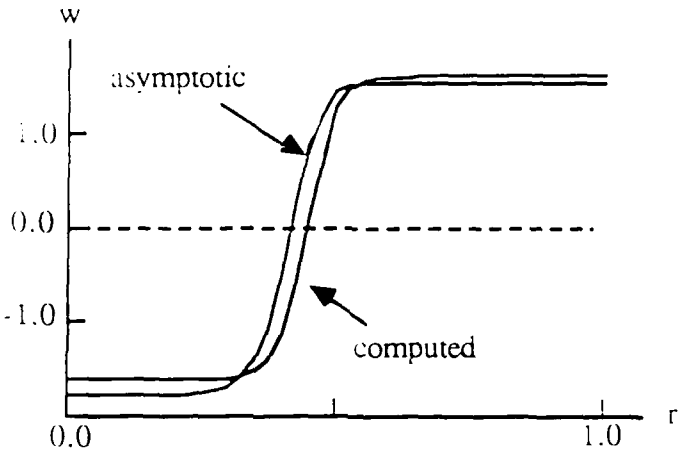
w
asymptotic
1.0
0.0
-1.0
computed
r
0.0
1.0

Figure

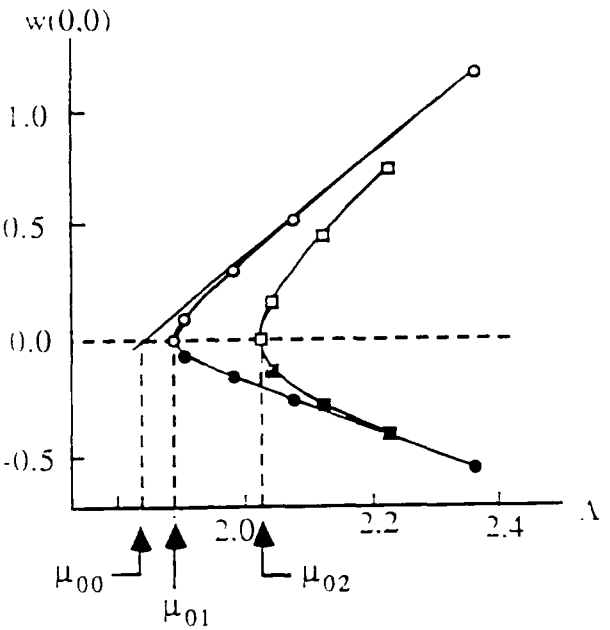

Figure 8

(a)

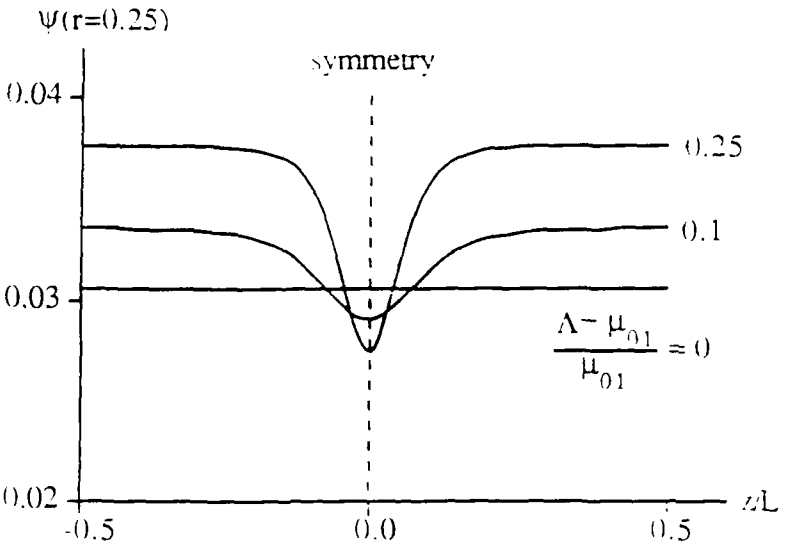
Ψ(r=0.25)
symmetry
0.04
0.03
0.02
0.25
0.1
$\frac{\Lambda - \mu_{01}}{\mu_{01}} = 0$
-0.5
0.0
0.5
z/L

(b)

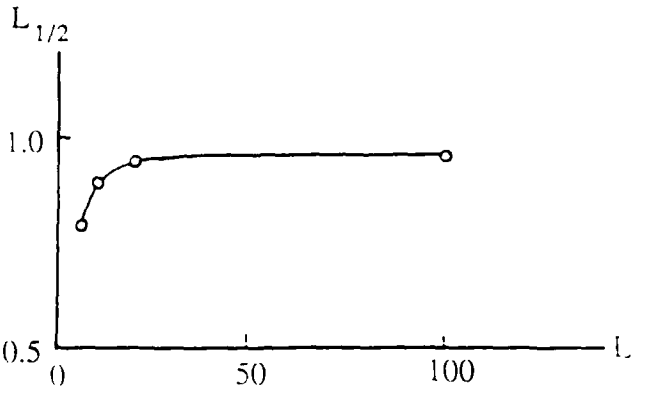
$L_{1/2}$
1.0
0.5
0
50
100
L

Figure 9

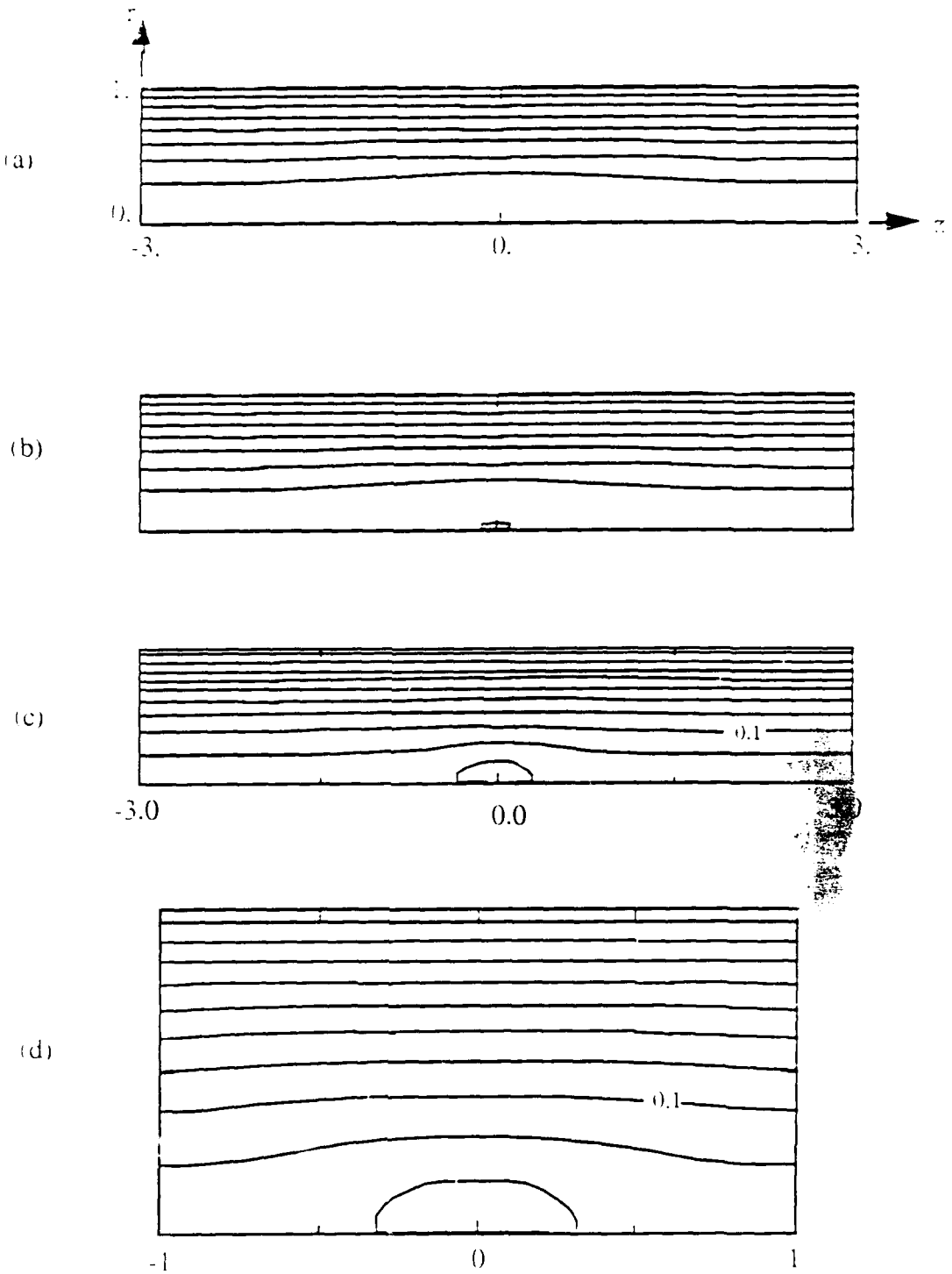

Fig 10

(a)

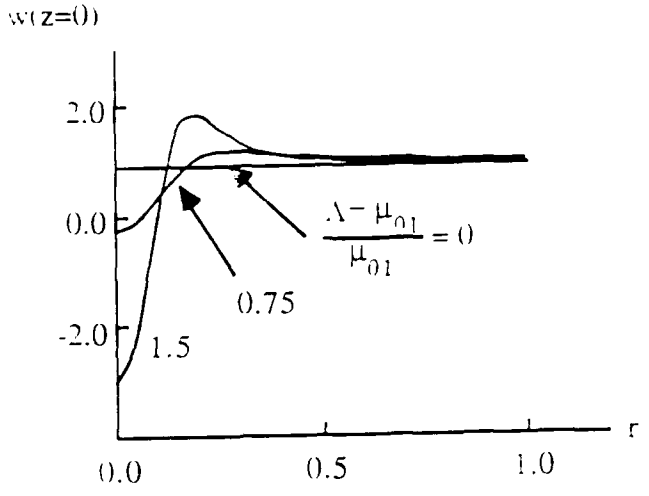
w(z=0)
2.0
0.0
-2.0
$\frac{\Lambda - \mu_{01}}{\mu_{01}} = 0$
0.75
1.5
r
0.0
0.5
1.0

(b)

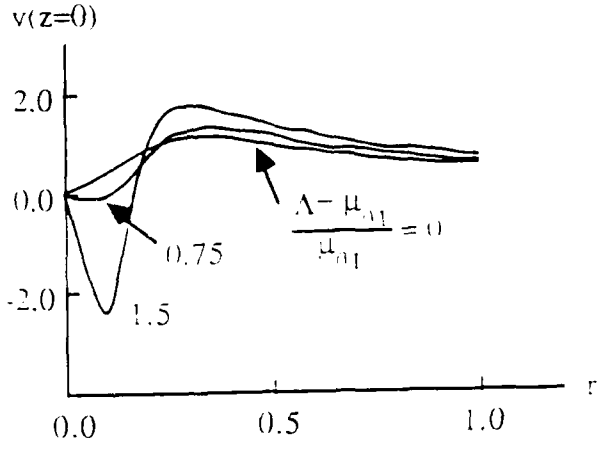
v(z=0)
2.0
0.0
-2.0
$\frac{\Lambda - \mu_{01}}{\mu_{01}} = 0$
0.75
1.5
r
0.0
0.5
1.0

Figure 11

(c)

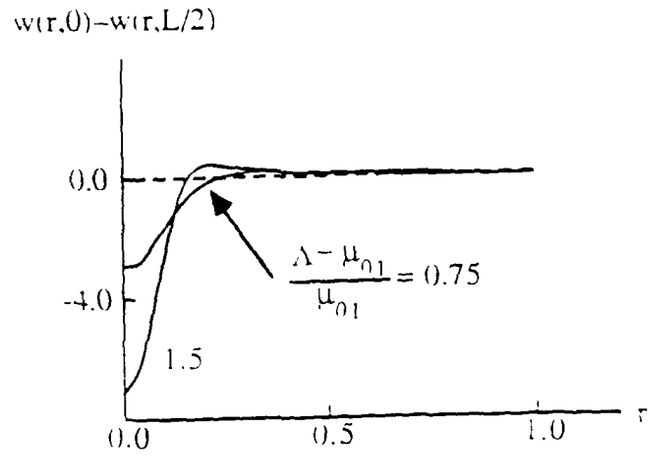

Figure 11 (continued)

(a)

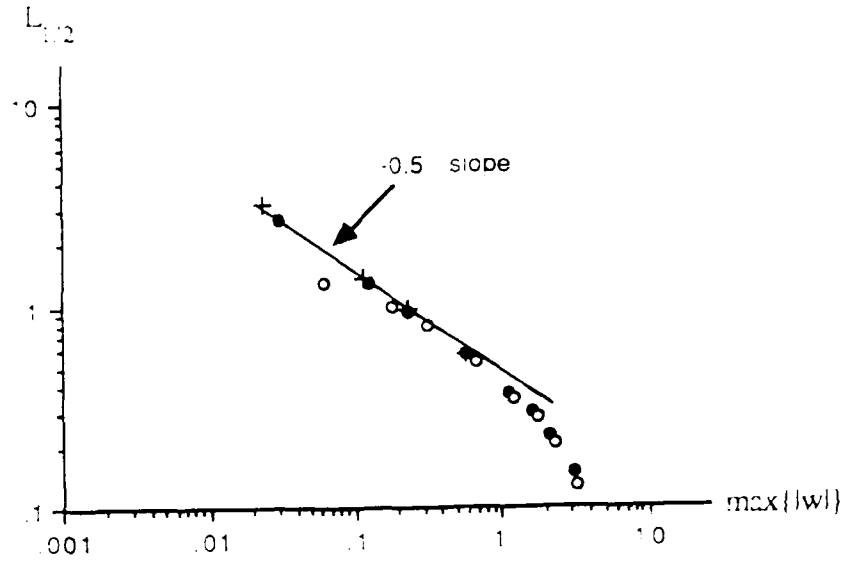
$L_{1/2}$
10
1
.1
-0.5 slope
.001
.01
.1
1
10
max{|w|}

(b)

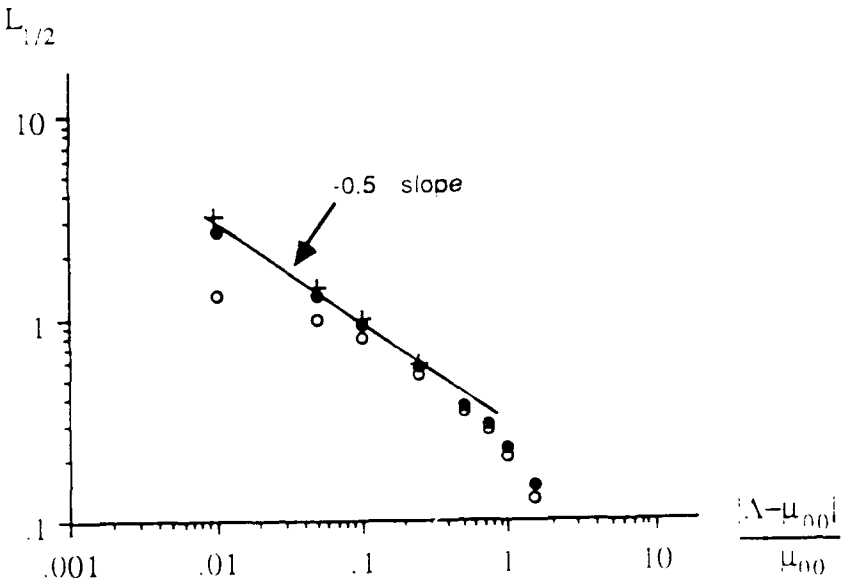
$L_{1/2}$
10
1
.1
-0.5 slope
.001
.01
.1
1
10
$\frac{|\Lambda-\mu_{00}|}{\mu_{00}}$

Figure 12

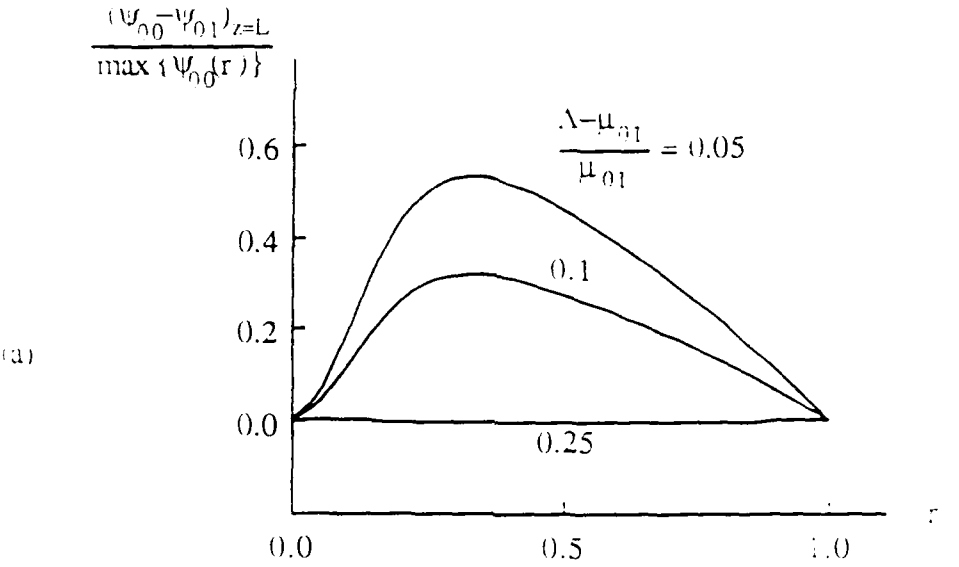
$\frac{(\Psi_{00}-\Psi_{01})_{z=L}}{\max\{\Psi_{00}(r)\}}$
0.6
0.4
0.2
0.0
$\frac{\Lambda-\mu_{01}}{\mu_{01}} = 0.05$
0.1
0.25
0.0
0.5
1.0
r

(a)

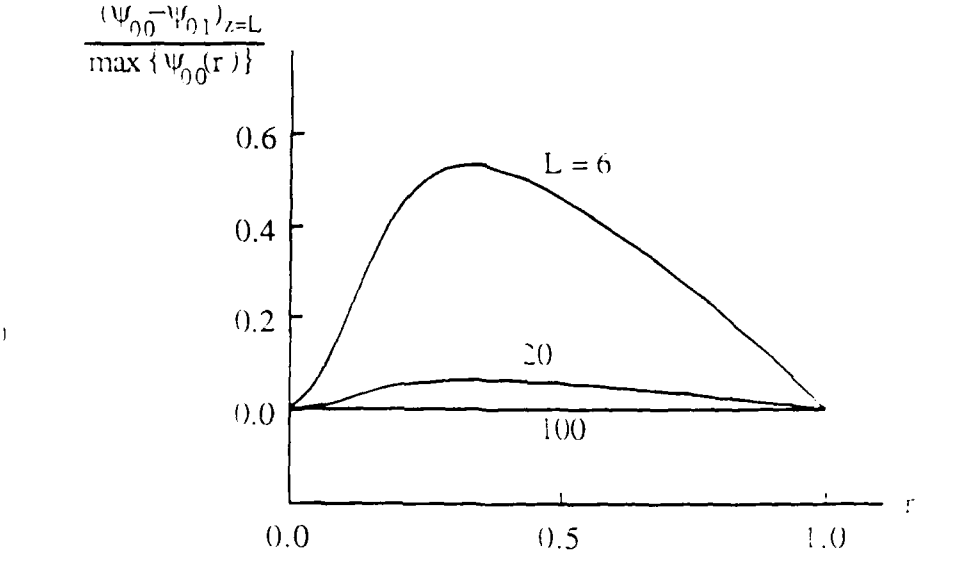
$\frac{(\Psi_{00}-\Psi_{01})_{z=L}}{\max\{\Psi_{00}(r)\}}$
0.6
0.4
0.2
0.0
L = 6
20
100
0.0
0.5
1.0
r

(b)

Figure 13

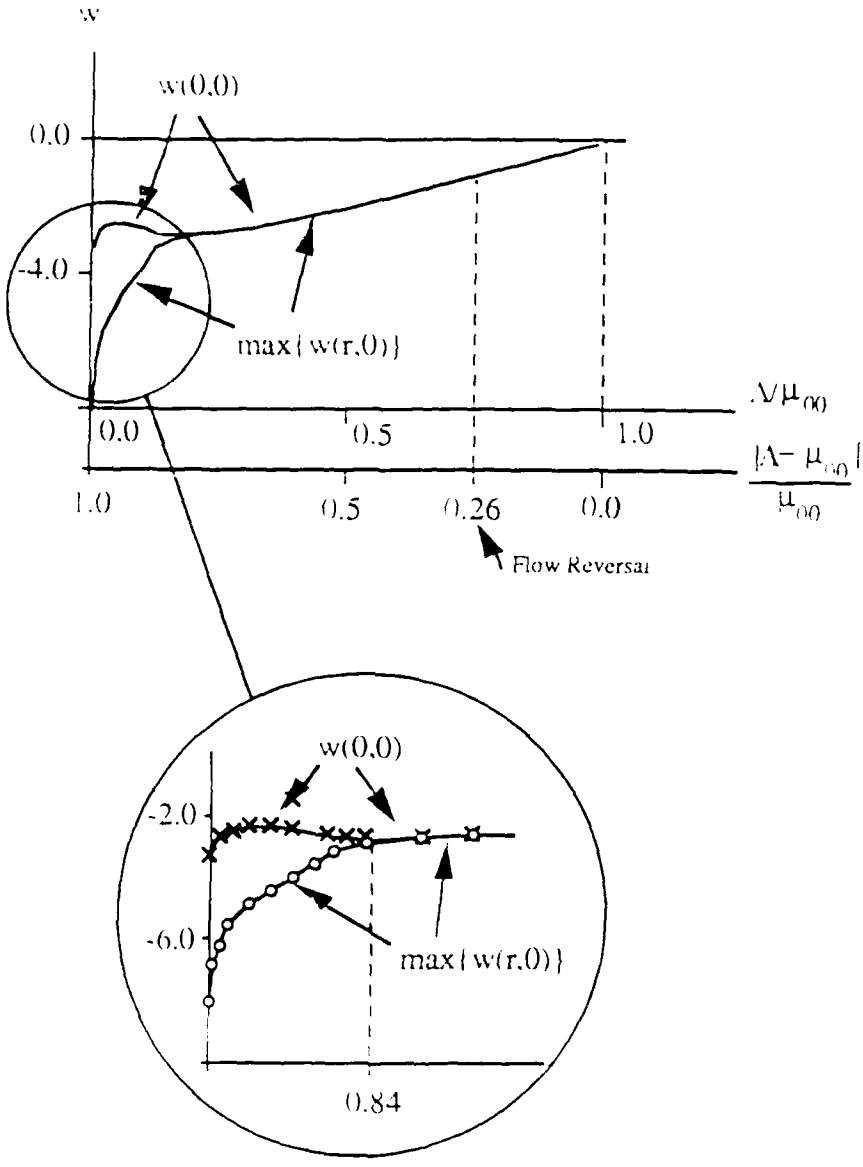
w
w(0,0)
0.0
-4.0
max{w(r,0)}
0.0
0.5
1.0
1.0
0.5
0.26
0.0
Flow Reversal
w(0,0)
-2.0
-6.0
max{w(r,0)}
0.84

Figure 14

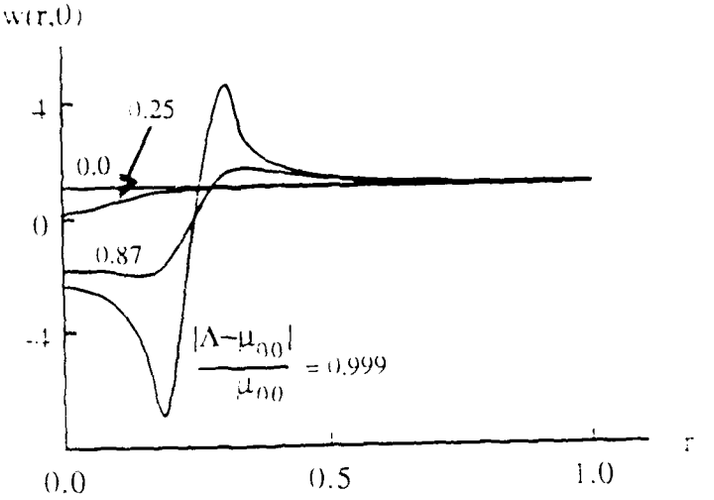

Figure 15

(a)

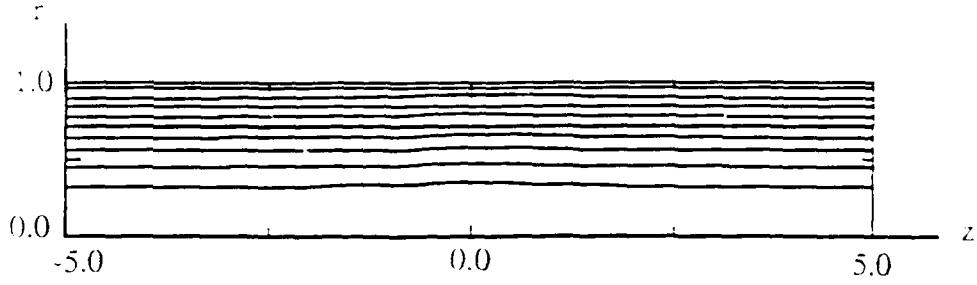

(b)

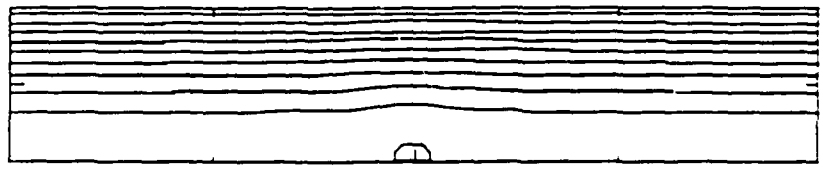

(c)

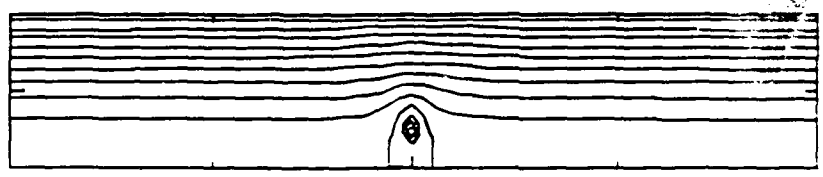

Figure 16

(d)

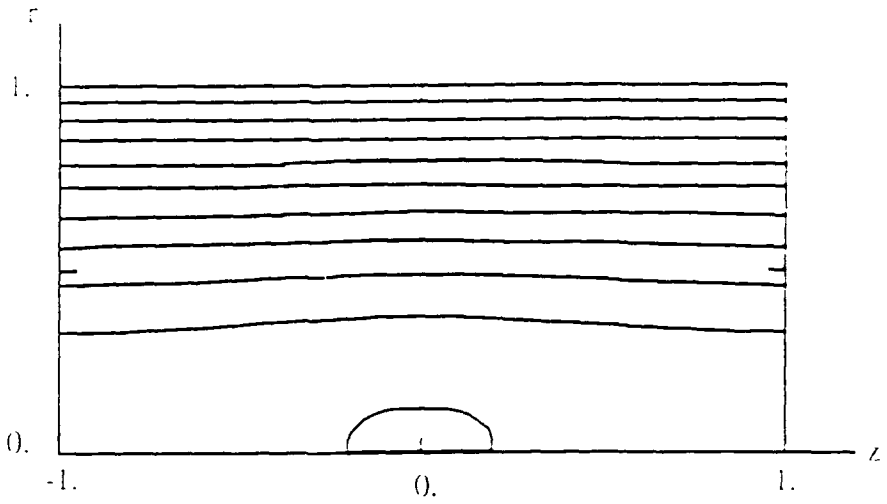

(e)

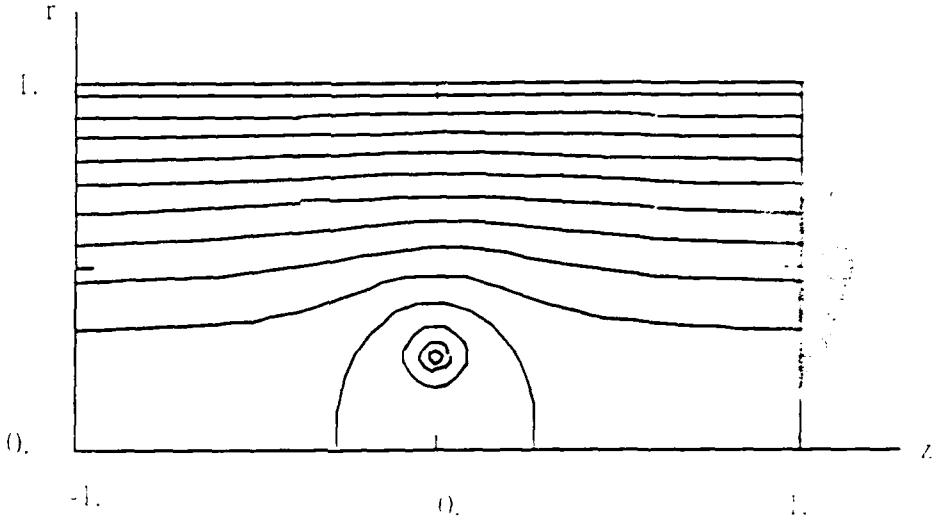

Figure 16 (continued)

(a)

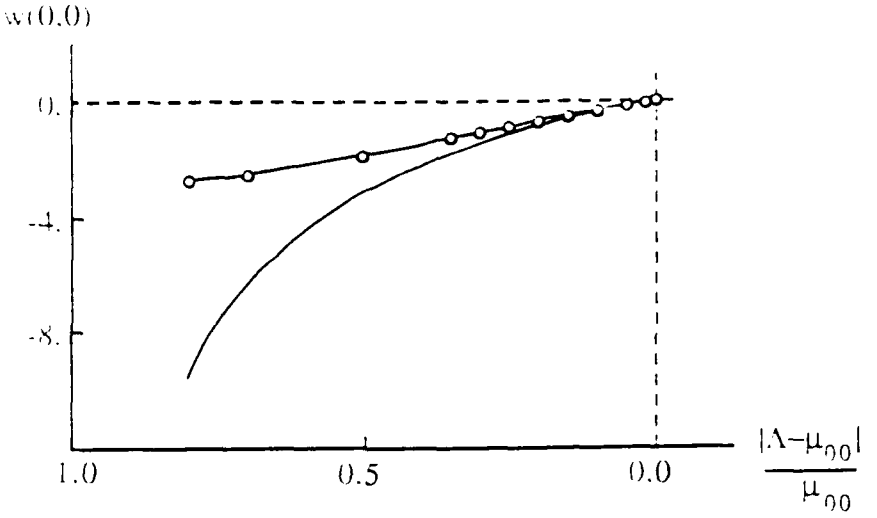
w(0,0)
0.
-4.
-8.
1.0
0.5
0.0
$\frac{|\Lambda-\mu_{00}|}{\mu_{00}}$

(b)

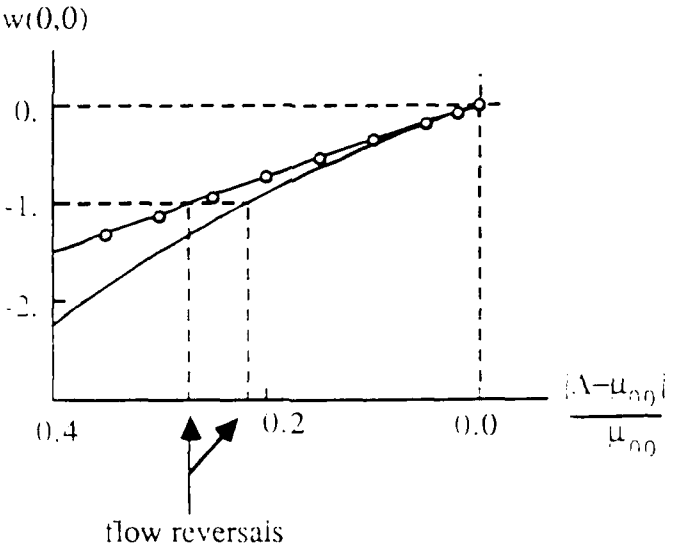
w(0,0)
0.
-1.
-2.
0.4
0.2
0.0
$\frac{|\Lambda-\mu_{00}|}{\mu_{00}}$
flow reversals

Figure 17

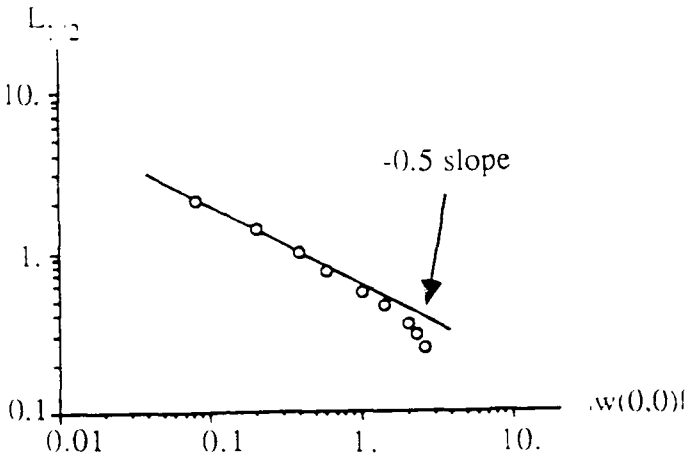

(c)

Figure 17 (continued)

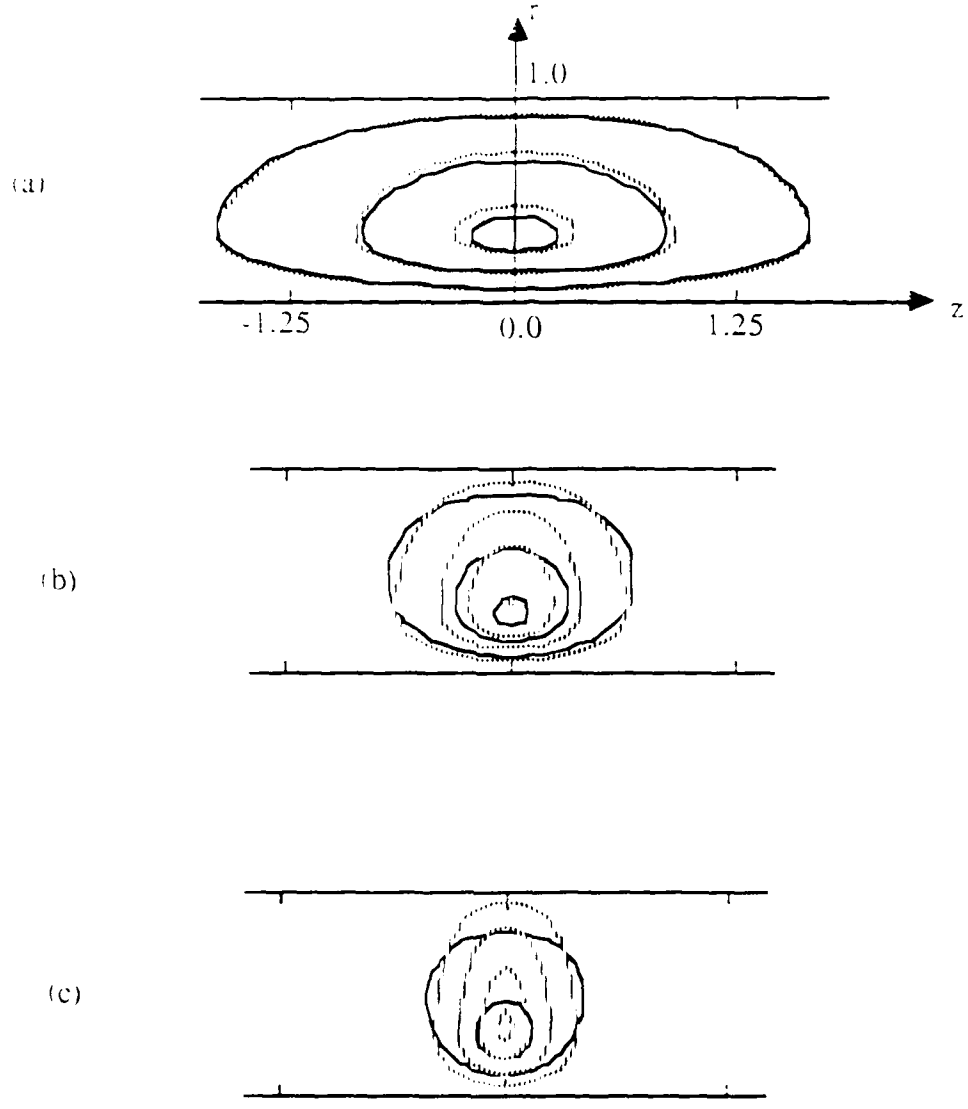

Figure 18

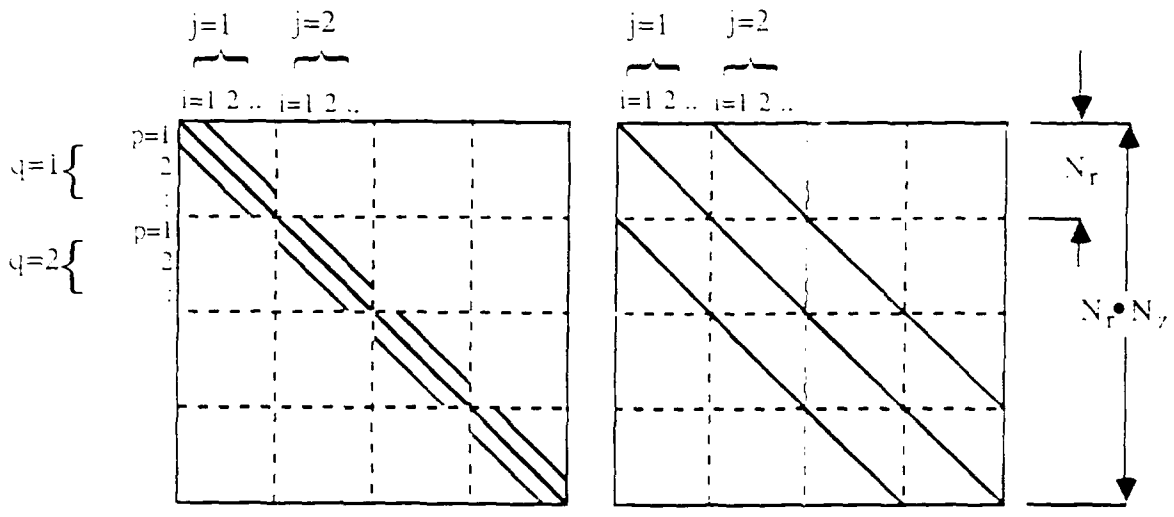

(a) (b)

Figure A1

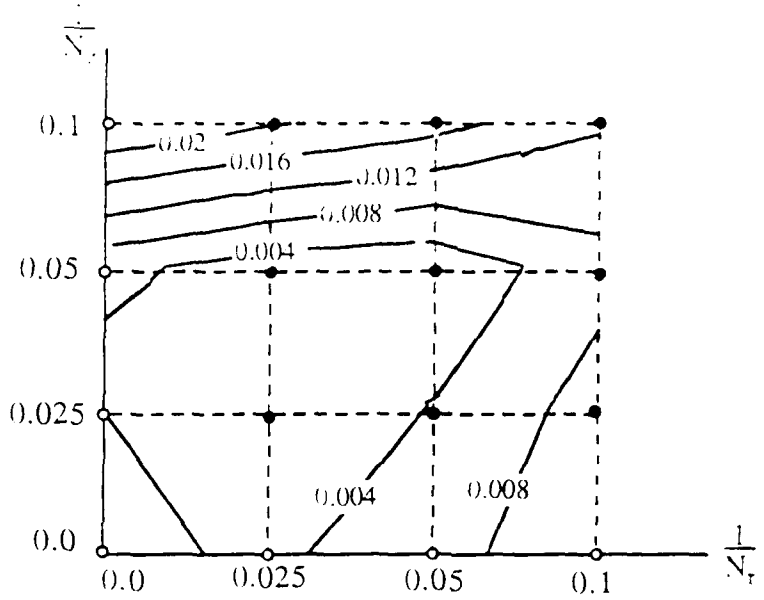
$\frac{1}{N_r}$
0.1
0.05
0.025
0.0
0.02
0.016
0.012
0.008
0.004
0.004
0.008
0.0
0.025
0.05
0.1
$\frac{1}{N_r}$

(a)

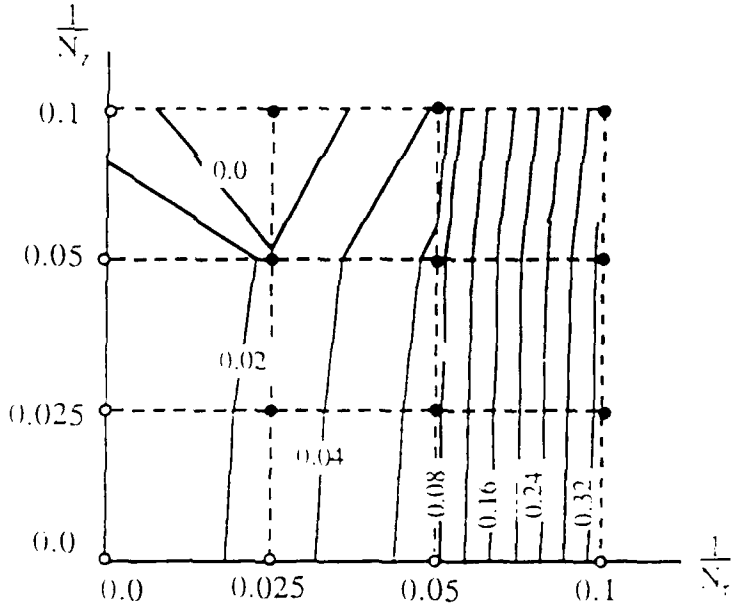
$\frac{1}{N_r}$
0.1
0.05
0.025
0.0
0.0
0.02
0.04
0.08
0.16
0.24
0.32
0.0
0.025
0.05
0.1
$\frac{1}{N_r}$

(b)

Figure A2

(c)

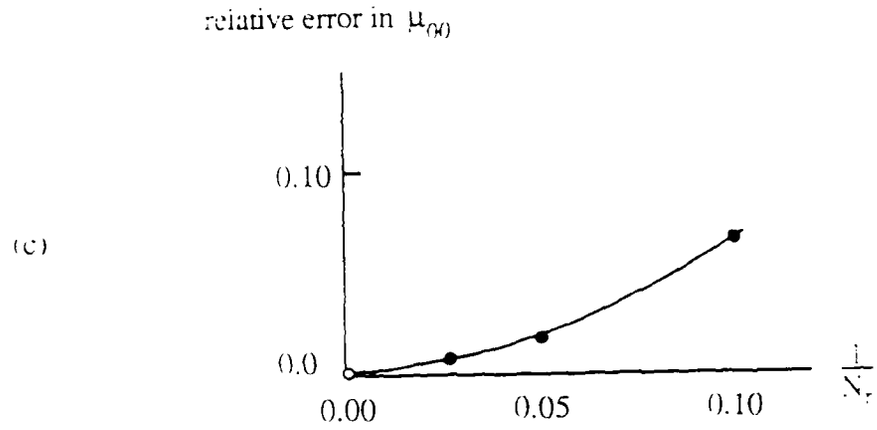

Figure A2 (continued)

(a)

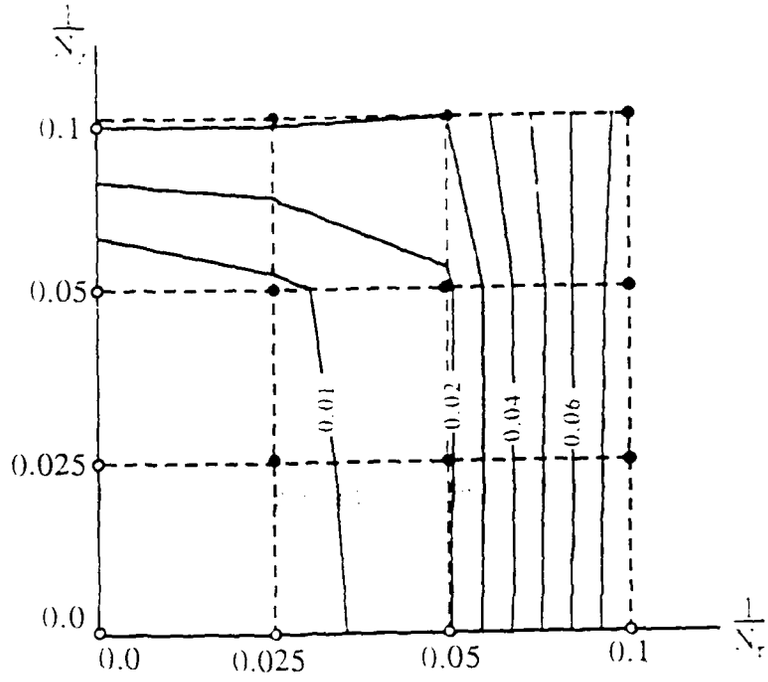
$\frac{1}{N_r}$
0.1
0.05
0.025
0.0
0.01
0.02
0.04
0.06
0.0
0.025
0.05
0.1
$\frac{1}{N_r}$

(b)

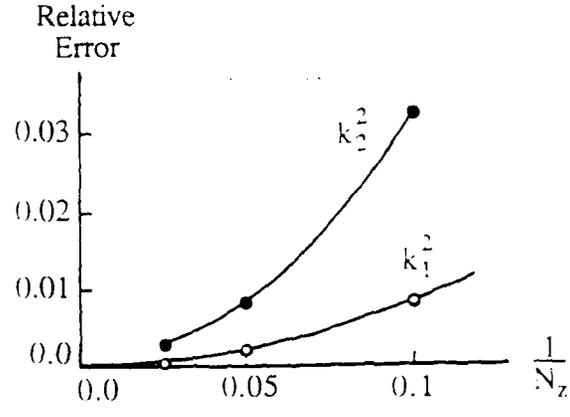
Relative Error
0.03
0.02
0.01
0.0
k_2^2
k_1^2
0.0
0.05
0.1
$\frac{1}{N_z}$

Figure A3

(c)

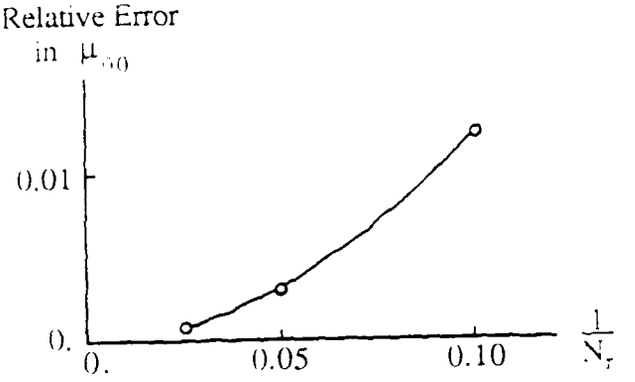

(d)

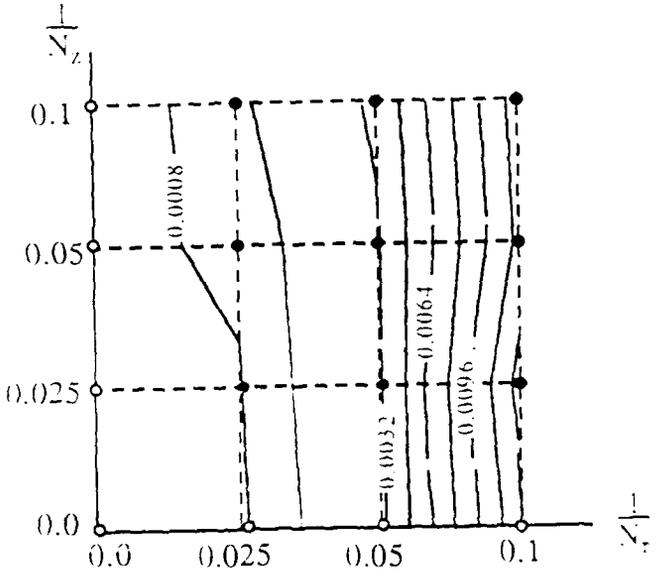

Figure A3 (continued)

Computation of Leading Eigenspaces for Generalized Eigenvalue Problems

Abraham Kribus
Mathematical Sciences Institute, Cornell University
Ithaca, NY 14853

Presented at the Seventh Army Conference
on Applied Mathematics and Computing
West Point, June 1989

A method for computing leading eigenvalues (having the largest real part) and their eigenvectors for large generalized eigenvalue problems is presented. A linear fractional transformation is used to map a group of leading eigenvalues into dominant eigenvalues (having the largest modulus). The Dominant eigenvalues of the transformed problem are computed by Stewart's (1976) Simultaneous Iteration. Each iteration involves matrix-vector multiplication and the solution of a linear system, which can be done efficiently if the matrices involved are sparse or have some special structure. Convergence properties are similar to those of the inverse power iteration: the method requires an estimate for the region in the complex plane containing the desired eigenvalues, and converges rapidly when a good estimate is available. The amount of work is also comparable to that of the basic inverse iteration, which is significantly less than that required for full eigensolution. Examples from hydrodynamic stability demonstrate convergence rates, computation time and the ability to resolve simultaneously groups of leading eigenvalues.

Computation of Leading Eigenspaces for Generalized Eigenvalue Problems

1. Introduction

A generalized eigenvalue problem has the form:

$$\mathbf{A}\,\mathbf{x} = \sigma\,\mathbf{B}\,\mathbf{x} \tag{1.1}$$

where $\mathbf{A}, \mathbf{B} \in \mathbb{C}^{n \times n}$ are general complex matrices. In many applications these matrices will have some useful structure, such as symmetry or sparsity.

Let the *Leading* Eigenvalues of (1.1) be those having the largest *real part* ; the more common term, *Dominant* Eigenvalues, refers to those having the largest *modulus* . In some applications, only a few leading eigenvalues of (1.1) are sought; for example, in hydrodynamic stability problems, the real part of σ is the growth rate, and the eigenvectors of the leading eigenvalues represent the most unstable modes.

Traditional methods for solving (1.1) usually involve finding all the eigenvalues, using the Q-Z algorithm (see IMSL or other numerical analysis libraries) and then sorting by the real part. This involves $O(n^3)$ work, where n is the order of the matrices, and becomes expensive or impractical for large n; little or no advantage can be taken of sparsity or other structure of **A** and **B**.

Several methods exist for extracting selected eigenvalues and eigenvectors of standard eigenvalue problems, i.e. when **B** is invertible (see, for example, Golub and Van Loan, 1983.) Power and Lanczos methods compute the dominant eigenvalues; inverse iteration can find the eigenvalues closest to a given point in the complex plane and their eigenvectors. These are not directly applicable to the problem of computing the leading eigenvalues.

Recently, an integration method was proposed (Goldhirsch *et al.* 1987) for the leading eigenvalues of a standard eigenvalue problem (where **B** is invertible.) This method is simple and elegant; however, its convergence may become very slow (or, alternatively, the size of the reduced problem may become too large) if the separation of the eigenvalues is small. Another problem may arise if the problem is defective, i.e. a leading eigenvalue has generalized eigenvectors; in this case, the integration method may return inconclusive or inconsistent results.

2. The Dominance Mapping Method

This method attempts to address the problems (1.1) which are not solved efficiently by the other methods mentioned above. It will work for singular **A** and **B**; for defective problems; it will take full advantage of the structure of the matrices; and it allows some control over convergence rates. There are a few restrictions, however, which will be discussed below.

The eigenvalues in the complex σ-plane can be mapped to a λ-plane by the linear fractional transformation:

$$\sigma = \beta + \alpha \frac{\lambda-1}{\lambda+1} \tag{2.1}$$

where α is a real positive, and β a complex, constant. The important effect of this linear fractional mapping is to map the half-plane to the left of $\sigma=\beta$ to the inside of the unit circle in the λ plane, as seen in fig. 1. If m leading eigenvalues are required, and we select β such that:

$$\mathrm{Re}(\sigma_i) \begin{cases} > \mathrm{Re}(\beta) & i=1\ldots m \\ < \mathrm{Re}(\beta) & i=m+1\ldots n \end{cases}$$

then the corresponding m eigenvalues will be *dominant* in the λ plane:

$$|\lambda_i| \begin{cases} > 1 & i=1\ldots m \\ < 1 & i=m+1\ldots n \end{cases}$$

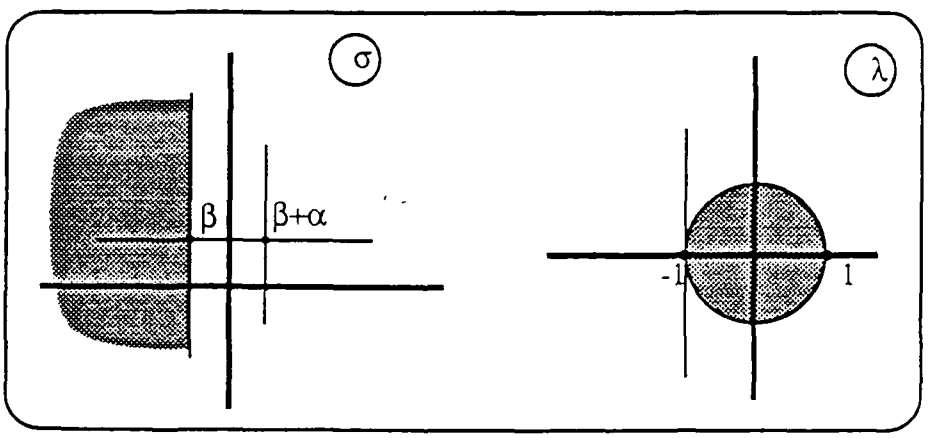

Figure 1: The Dominance Mapping (2.1)

The eigenvalue problem for λ is in standard form:

$$\mathbf{C}\,\mathbf{u} = \mathbf{C}_1^{-1}\,\mathbf{C}_2\,\mathbf{u} = \lambda\,\mathbf{u} \tag{2.2}$$

where:

$$C_1 = - [A-(\alpha +\beta) B]$$

$$C_2 = [A+(\alpha -\beta) B]$$

The problem of computing the leading eigenvalues of (1.1) becomes that of computing the dominant eigenvalues of (2.2); the methods mentioned in §1 can now be applied. We used Stewart's (1976) version of Simultaneous Iteration, which applies to the most general, non-hermitian C.

A transformation similar to (2.1) was proposed by Jennings (1977), in the context of converting a quadratic eigenvalue problem to standard form. Jennings (and no one else, to the best of the author's knowledge) has not made the second step of applying a dominant eigenvalue method to a transformed problem equivalent to (2.2).

The mapping constants α and β allow the user some control over the rate of convergence and the order in which the leading eigenvalues emerge during the iteration. The user must have an estimate of where in the complex plane the leading eigenvalues reside; β is set to the left of this region. The point $c = \beta+\alpha$ is a singular point of (2.1) which maps to infinity in the λ plane; eigenvalues close to c will map to very large modulus in the λ plane, and will converge rapidly during the iteration of (2.2). α should be set, therefore, so that c is near the center of the leading region or near the most important eigenvalue.

The following algorithm computes m leading eigenvalues and eigenvectors of (1.1), using the Dominance Mapping:

1. estimate leading region; select α , β
2. perform L-U decomposition of $C_1 = - [A-(\alpha +\beta) B]$;
   (use the structure of A and B)
3. select m initial column vectors $\mathbf{u}^{(0)} \in \mathbb{C}^{n \times m}$
4. Simultaneous Iteration on $C u = \lambda u$:
   for each multiplication $\mathbf{u}^{(k+1)} = C \mathbf{u}^{(k)}$ do:
   4.1 multiply: $\mathbf{v} = C_2 \mathbf{u}^{(k)}$
   4.2 solve the system: $C_1 \mathbf{u}^{(k+1)} = \mathbf{v}$
5. map converged $\lambda_i \rightarrow \sigma_i$.

3. Singularities in the Dominance Mapping

The algorithm of §2 may fail in two cases, corresponding to the two singularities of the mapping (2.1): the point $\sigma=c$, which maps to infinity in λ, and $\lambda=-1$ which maps to infinity in σ.

When $|c - \sigma_i| < \varepsilon$ for some $i \leq m$, for a small (machine-dependent) ε, then the matrix C will be ill-conditioned or numerically singular. This is easily remedied by a small change in α, which does not significantly affect any other properties of the mapping.

When $|\mathrm{Im}(\sigma_i - c)| \gg 1$ for some $i \leq m$, the corresponding λ-eigenvalue is close to the singular point $\lambda=-1$. This implies that its separation from the subdominant eigenvalues inside the unit circle is small, often so small that convergence is impractical. Some improvement may result if we increase α; but this may decrease the modulus of other dominant λ-eigenvalues and slow down their convergence. In a case where leading eigenvalues are widely separated in the imaginary direction, it may be necessary therefore to restart the iteration with different β values to resolve separate clusters of leading eigenvalues.

4. Example:

The performance of the DM method can be demonstrated by observing the amount of work needed to resolve a fixed subset of leading eigenvalues, as the order of the problem increases. The following example includes tridiagonal matrices of increasing size N, all having two leading eigenvalues:

$$\begin{aligned} &\sigma_1 = 1.2 \\ &\sigma_2 = 1.1 \\ &\mathrm{Re}(\sigma_i) \leq 1 \qquad \text{for } i = 2...n\,. \end{aligned} \tag{4.1}$$

Selecting $\alpha = 0.3$, $\beta = 1.0$ isolates σ_1, σ_2 . The problem was solved first using the traditional QZ routines (IMSL), then using the DM method but treating the matrices as dense, and finally taking full advantage of the structure. The results are shown in Figure 2.

The savings in computing time relative to the full eigensolution can be significant: at $n = 100$, only $\frac{1}{5}$ of the work is necessary even without exploiting the band structure; the work is reduced by more than an order of magnitude when the structure is used.

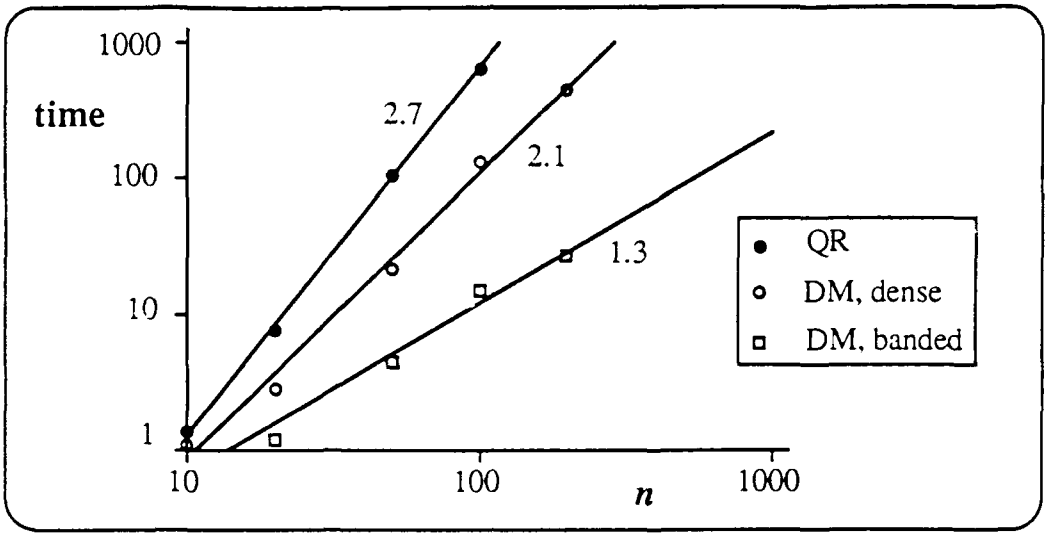

Figure 2: Comparison of work to resolve 2 leading eigenvalues of (4.1)

5. Application to the Orr-Sommerfeld Equation

The Orr-Sommerfeld equation:

$$(D^2 - \alpha^2)^2 \psi = i\alpha R \left[(U-c)(D^2-\alpha^2)\psi - U''\psi \right] \qquad (5.1)$$

describes the hydrodynamic stability of parallel shear flow (see, for example, Drazin and Reid 1981.) High accuracy eigenvalues were computed by Orszag (1971) for plane Poiseuille flow with R=10000 (Reynolds number) and α=1 (streamwise wavenumber.) The location of the twelve least stable eigenvalues are shown in figure 3.

Equation (5.1) is discretized using central differences (a spectral method may be more appropriate in this specific case, as in Orszag (1971), but the banded finite-difference matrix is a good example of candidate problems for the DM method.) The eigenvalue c is replaced by σ=-ic , to conform with the definitions of (1.1).

When Im(β)≈Im(σ_1), eigenvalues 1 and 4 were the first to converge; 2, 3, 5 and 6 took longer .) converge, since the imaginary part separation brought their λ counterparts close to the singular point λ=-1. For Im(β)≈Im(σ_2), the order was reversed: first eigenvalues 2, 3, 5 and 6 and then 1 and 4. In both cases, the first group converged within 10 to 15 iterations, regardless of the number of grid points.

The error associated with convergence of the λ-iteration was not significant in our computations. Using a stopping criterion of $\|\mathbf{Cu}-\lambda\mathbf{u}\| \le 10^{-3}$, the leading σ-eigenvalues were converged to at least 5 digits. The discretization error of the finite-differencing (compared to Orszag's results) is proportional to Δx^2, as expected. The time to resolve the

most unstable eigenvalue and its discretization error vs. the grid resolution are plotted in figure 4.

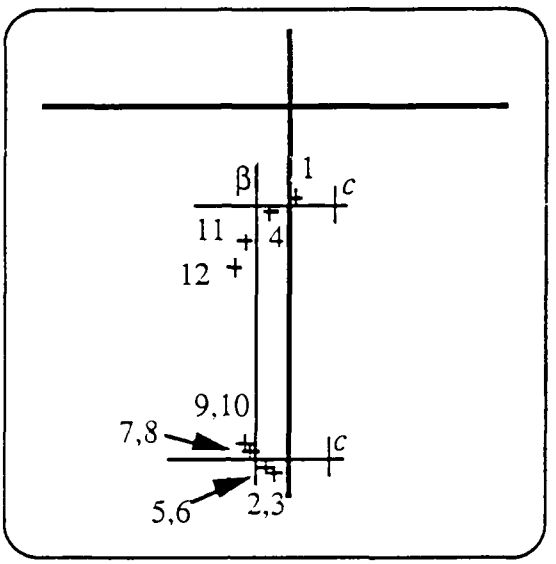

Figure 3: Poiseuille flow eigenvalues. R=10000, α=1.0

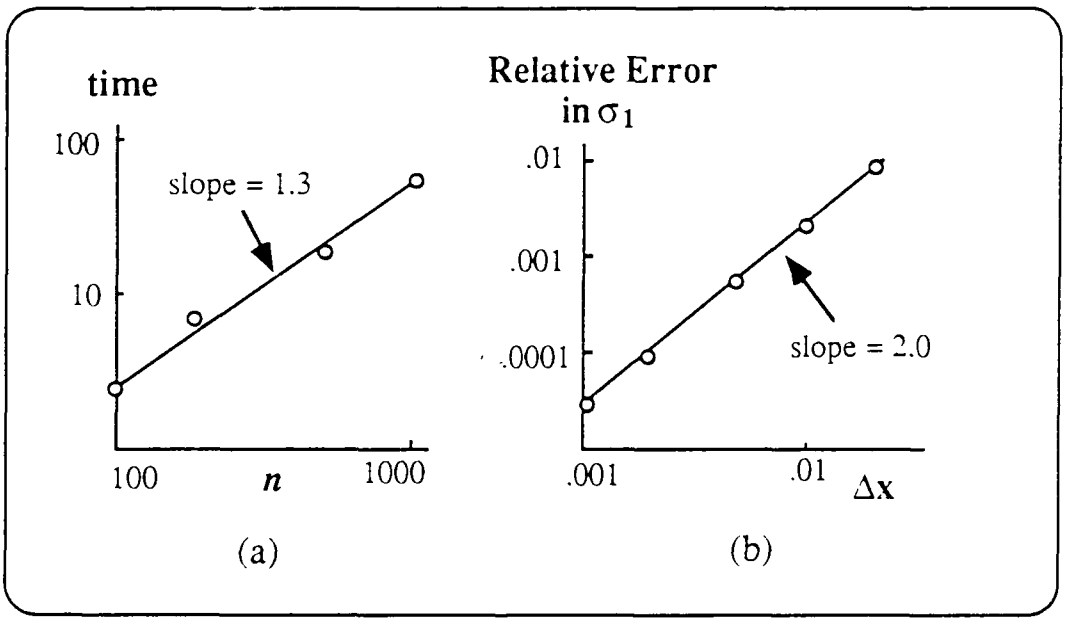

Figure 4: (a) the time to compute the most unstable eigenvalue of (5.1)
(b) discretization error vs. the grid interval Δx

6. Conclusion

Using the Dominance Mapping and a Power Iteration method we can compute leading eigenvalues and eigenvectors of large generalized eigenvalue problems. This method can be more efficient than a full eigensolution even for a general pair of matrices, but is especially attractive when the matrices have a structure that can save work in the Gaussian elimination and matrix multiplication steps. The DM method can be applied to singular and defective problems that may cause failure or slow convergence in other methods.

Use of the DM method is restricted, however, to cases where an estimate for the leading eigenvalues is available. When this estimate shows a wide distribution of leading eigenvalues along the imaginary direction, several passes may be necessary with different mapping parameters to properly resolve all leading eigenvalues, as demonstrated for the Orr-Sommerfeld problem.

Acknowledgement

This work was supported by the U. S. Army Research Office Mathematical Sciences Institute at Cornell University and by the Air Force Office of Scientific Research under contract AFOSR-87-0255.

References

Drazin, P.G. and Reid, W.H. (1981). *Hydrodynamic Stability*, Cambridge University Press, New York.

Goldhirsch, I., Orszag, S.A., and Maulik, K. (1987). *An Efficient Method for Computing Leading Eigenvalues and Eigenvectors of Large Asymmetric Matrices* , J. Sci. Comput. **2**(1) , 33.

Golub, G.H. and Van-Loan, C.F. (1983). *Matrix Computations* , The Johns Hopkins University Press, Baltimore.

Jennings, A. (1977). *Matrix Methods for Engineers and Scientists*, John Wiley & Sons, Chichester.

Orszag, S.A. (1971). *Accurate Solution of the Orr-Sommerfeld Stability Equation* , J. Fluid Mech. 50, 689-703.

Stewart, G.W. (1976). *Simultaneous Iterations for Computing Invariant Subspaces of Non-Hermitian Matrices* , Numer. Math. **25**, 123.